

Bringing Your Portrait to 3D Presence

Jiawei Zhang^{1†} Lei Chu² Jiahao Li² Zhenyu Zang² Chong Li²
 Xiao Li² Xun Cao¹ Hao Zhu¹ Yan Lu²

¹Nanjing University ²Microsoft Research Asia

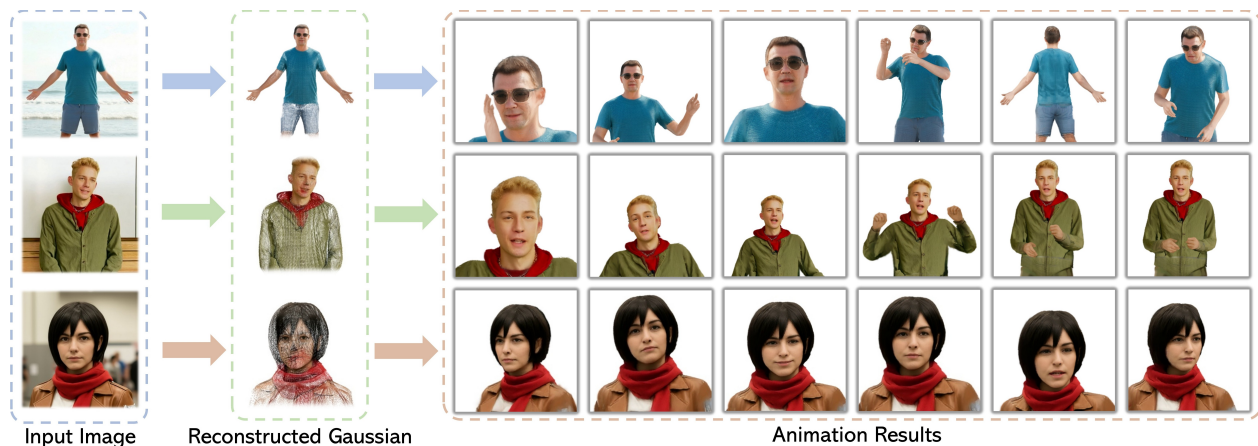


Figure 1. Our method uses a dual-UV formulation to represent 3D avatars, enabling reconstruction from full-body, half-body, and headshot portraits while capturing off-body textures. Trained entirely on synthetic data, it generalizes effectively to in-the-wild images.

Abstract

We present a unified framework for reconstructing animatable 3D human avatars from a single portrait across head, half-body, and full-body inputs. Our method tackles three bottlenecks: pose- and framing-sensitive feature representations, limited scalable data, and unreliable proxy-mesh estimation. We introduce a Dual-UV representation that maps image features to a canonical UV space via Core-UV and Shell-UV branches, eliminating pose- and framing-induced token shifts. We also build a factorized synthetic data manifold combining 2D generative diversity with geometry-consistent 3D renderings, supported by a training scheme that improves realism and identity consistency. A robust proxy-mesh tracker maintains stability under partial visibility. Together, these components enable strong in-the-wild generalization. Trained only on half-body synthetic data, our model achieves state-of-the-art head and upper-body reconstruction and competitive full-body results. Extensive experiments and analyses further validate the effectiveness of our approach.

[†]This work was done during Jiawei Zhang’s internship at Microsoft Research Asia.

1. Introduction

Creating animatable 3D human avatars is central to telepresence and virtual reality. While high-quality avatars usually rely on multi-view capture or depth sensors, these setups limit scalability; reconstructing an animatable avatar from a single portrait offers a far more accessible solution.

Despite rapid progress in 3D human reconstruction, most existing methods are designed either for head-only or for full-body avatars, and often rely on specific input assumptions. In particular, many pipelines assume full-body visibility (including both hands and feet) to obtain stable proxy mesh (e.g., SMPL-X [66], FLAME [51]) fitting, an assumption that is not always satisfied in real scenarios, where upper-body or partial views are more typical. Recent transformer-based frameworks, including the Large Avatar Model [28] (LAM) and Large Human Model [71] (LHM), follow the Large Reconstruction Model [32] (LRM) paradigm by encoding input images into patch-level features and using learnable tokens to query them through cross-attention. This design enables fast single-image reconstruction without explicit geometry or texture optimization but constrains the representation to the image feature space, making it difficult to generalize across incomplete inputs. As shown in LHM, performance

degrades under pose variation or partial-body inputs, and even when trained on half-body data, the ambiguous definition of “half-body,” ranging from shoulder to waist or thigh crops, leads to inconsistent spatial correspondence and noticeable quality drops compared to full-body cases. Our goal is to relax both input and data requirements, advancing toward in-the-wild 3D avatar reconstruction from everyday captures such as webcams or phone portraits, thereby extending the scalability of animatable avatar reconstruction beyond controlled environments.

Our investigation reveals that the fundamental obstacles to advancing single-image 3D avatar reconstruction arise primarily from three aspects. First, **representation design**. Most existing pipelines inherit ViT-based pretrained encoders, which lack strict translation invariance and thus require the input image to be spatially aligned to a fixed reference. Unlike general object reconstruction, human images exhibit large pose variations and frequent partial-body visibility, making such alignment inherently unstable. Consequently, the decoder must learn to correlate image patches with 3D representations while adapting to token distribution shifts induced by pose and alignment inconsistencies, often leading to identity drift and texture distortion. Second, **data scalability**. High-quality multi-view human datasets require expensive studio setups with synchronized cameras, whereas real monocular videos demand intensive manual cleaning to ensure temporal and pose consistency. Synthetic data from traditional rendering engines offer controllable geometry but limited appearance diversity and a large domain gap to real imagery. Although 2D generative models can produce photorealistic humans with diverse appearances, their results generally lack identity and cross-view consistency, making them unsuitable for 3D supervision without further processing. Third, **robust body estimation**. Reliable proxy mesh tracking remains a key bottleneck. Existing trackers often assume full-body visibility, some even require both hands or the entire silhouette, to stabilize optimization, which rarely holds in in-the-wild captures dominated by upper-body views.

To address these challenges, we present a unified pipeline that integrates representation design, data construction, and proxy mesh estimation in a coherent framework. (1) **Dual-UV Representation**. At the core of our system is a Dual-UV representation that rearranges image features into a continuous, geometry-aligned UV space. It comprises two complementary branches: a Core-UV that encodes on-surface, geometry-anchored features, and a Shell-UV that captures off-surface details such as hair, clothing, and accessories by sampling features on an offset mesh shell. By anchoring tokens to a canonical surface rather than image coordinates, it eliminates token-distribution shifts caused by pose and alignment variations, which often lead to identity drift and texture distortion. This enables a sin-

gle model to robustly handle head-only, half-body, and full-body inputs within one framework. (2) **Factorized Synthetic Data Manifold**. Our model is trained entirely on synthetic data that combines 2D generative and 3D rendered sources to achieve both appearance diversity and geometric reliability. Rather than enforcing multi-view consistency on 2D generative models, we leverage their ability to produce diverse, photorealistic appearances resembling real imagery. The 3D renderings, though less realistic, provide consistent geometric supervision that anchors reconstruction. All data are organized within a factorized, controllable manifold defined by semantically interpretable factors. A tailored training scheme mitigates identity and cross-view inconsistencies in the 2D data, while a realism regularizer projects each sample into a physically coherent, filmic space, preserving diversity while enhancing plausibility. Together, these designs yield a scalable synthetic corpus that enables stable training and strong generalization to in-the-wild captures. (3) **Proxy Mesh Estimation**. We empirically identify a stable configuration for human proxy mesh tracking under varying input completeness. Unlike previous approaches requiring full-body or both-hand visibility, our tracker maintains reliable performance across head-only, half-body, and full-body inputs, lowering capture demands and improving data scalability.

In summary, our work advances single-image 3D avatar reconstruction through the following contributions:

- We propose a simple yet effective Dual-UV representation that maps all inputs into a continuous, geometry-aligned UV space, enabling a single model to handle head-only, half-body, and full-body views.
- We construct a factorized synthetic data manifold with rich appearance diversity and controllable structure, supported by a training scheme that reduces identity inconsistency and cross-view mismatch, enabling strong real-world generalization from synthetic data alone.
- We develop a robust proxy-mesh tracker that remains stable across varying input completeness, reducing dependency on full-body visibility and improving scalability for in-the-wild reconstruction.
- Trained solely on half-body data, our approach achieves state-of-the-art head and upper-body results and competitive full-body performance. Code will be released upon acceptance.

2. Related Work

2.1. Human Datasets

Large-scale datasets underpin modern human modeling and fall into two categories. Structured datasets [27, 105] use controlled multi-view capture and provide diverse expressions, poses, and lighting [8, 13, 15, 34, 42, 58, 81, 84, 97, 102]. They support factor disentanglement but are

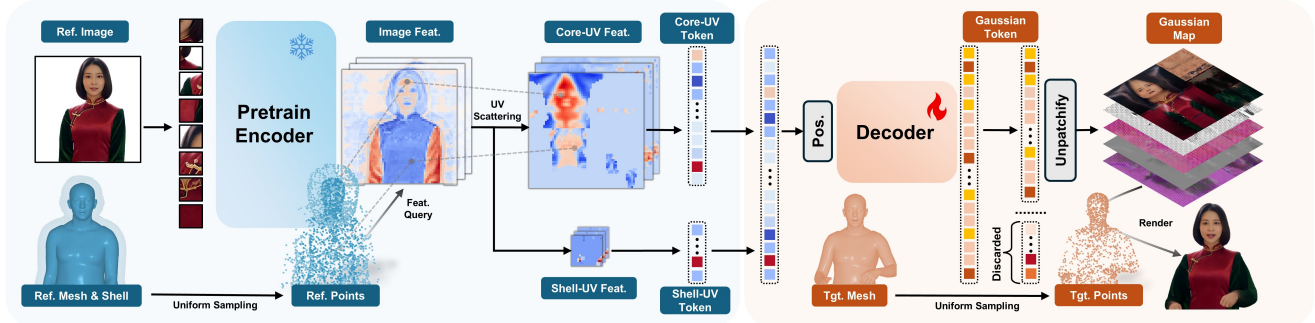


Figure 2. **Reconstruction Pipeline.** Given a reference image and its tracked proxy mesh, dense features from a frozen encoder are sampled along visible rays and scattered into canonical UV space to form the Core-UV map, while an offset shell captures off-surface regions such as hair and clothing. The Core-UV and Shell-UV tokens are fused and decoded by a lightweight transformer to reconstruct UV-space Gaussian attributes, which are then rigged to a target mesh and rendered from arbitrary viewpoints.

costly and limited to studio environments. Unstructured datasets [12, 21, 35, 38, 48, 96] collect in-the-wild images and videos with broad identity coverage but suffer from strong viewpoint bias toward near-frontal shots.

A complementary direction builds synthetic datasets [29, 88, 103] by rendering detailed assets with accurate annotations. They offer high controllability but exhibit realism and texture gaps relative to real imagery. Recent generative models [19, 23, 74, 114] help narrow this gap, enabling large-scale, realistic, and diverse synthetic human data. IDOL [114] also leverages 2D generative models for data curation by finetuning them for multi-view synthesis, but this introduces bias to the data diversity and still lacks reliable geometric consistency. In contrast, we retain the raw texture richness and diversity of 2D generative data without relying on its multi-view validity.

2.2. Head and Body Modeling

3D human modeling spans head and full-body reconstruction, following a similar evolution. Early methods recovered geometry with explicit meshes or implicit fields [75, 98, 99, 110], and neural rendering [39, 59] shifted the focus to high-fidelity appearance. 3D-aware GANs [10, 11] enabled controllable head [2, 43, 46, 47, 104, 106] and body [1, 18, 30, 109] synthesis, often leveraging 3DMM priors [5]. Score-distillation [69] further allowed diffusion-driven generation of diverse 3D humans [44, 56, 77, 89, 95, 113].

A complementary line learns person-specific avatars from studio captures [17] or monocular videos [9]. For heads, studio setups enable generalizable models [26, 31, 49], and per-subject optimization achieves high fidelity [7, 70, 76, 94, 95, 100, 108, 111, 112]. For bodies, appearance and clothing variability make generalization harder, so many works rely on per-subject fitting from monocular [25, 60, 68] or multi-view captures [6, 52, 65, 87, 101].

More recent efforts use multi-view [14, 33, 37, 50] and video-diffusion models [36, 57, 73] to generate multi-view imagery and reconstruct 3D avatars. In parallel, meth-

ods [28, 71] based on large reconstruction models [32, 86] provide single-forward 3D inference.

Recent works [1, 43, 49, 114] also use UV space for avatar attribute, but rely on StyleGAN or cross-attention to modulate UV attributes. We instead employ a non-learnable, closed-form projection from image space to UV space, enabling faithful texture transfer and strong identity preservation without generative hallucination.

2.3. Portrait Modeling

Upper- or half-body avatar modeling from casual inputs is relatively underexplored and remains challenging. It must preserve head-level facial detail while also handling arm articulation and clothing, yet unlike full-body settings, it demands higher facial fidelity and expression consistency.

Existing half-body approaches are limited: many depend on fixed multi-view capture for real-time systems [45, 82], while others only extend head models slightly toward the shoulders [22, 90–93]. While diffusion-based methods [24, 53, 55] generate person-specific upper-body avatars but are generally constrained to frontal poses and do not generalize well to wider viewpoints. Recently, GUAVA [107] achieved a generalizable upper-body Gaussian avatar. GUAVA also uses a UV branch for appearance, but unlike our dual-UV design, it relies on a separate template branch to encode the input, and stabilize the training process, thus requires a later refining module to blend the Gaussians from two branches.

3. Method

Given a single RGB portrait I , our goal is to reconstruct an *animatable* 3D human avatar represented by a set of Gaussians $\mathcal{G} = \{g_i = (\mu_i, \Sigma_i, c_i, \alpha_i)\}_{i=1}^N$. We decompose the latent space into two complementary parts: $\mathbf{z} = \{\mathbf{z}_{uv}, \mathbf{z}_{mesh}\}$, where \mathbf{z}_{uv} is a *dual-UV representation* encoding geometry-aligned appearance and visibility in a canonical UV space, and \mathbf{z}_{mesh} is a *proxy mesh latent* parameterized by proxy mesh to capture pose-dependent deformation.

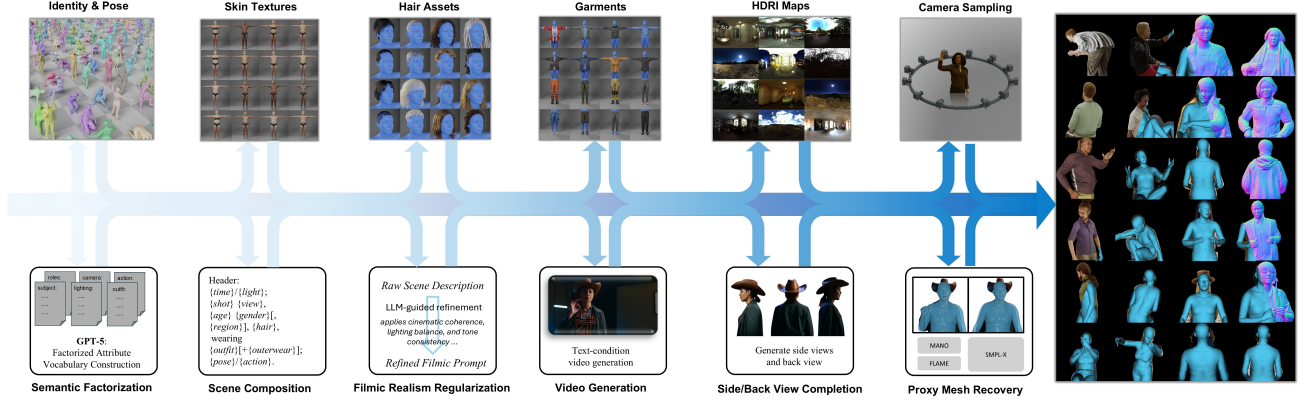


Figure 3. **Data Curation.** We build a hybrid dataset by combining geometry-anchored 3D rendering with semantics-driven generative synthesis. The *synthetic rendering branch* offers geometry-consistent multi-view supervision through procedural sampling of identity, pose, appearance, illumination, and cameras. The *generative branch* constructs a factorized appearance manifold by decomposing scene attributes, applying LLM-based filmic refinement, generating photorealistic sequences, and completing each sample with side/back views for weakly correlated augmentation.

The overall mapping is formulated as

$$f_{\theta} : I \rightarrow \mathbf{z}_{UV}, \quad \mathcal{G} = \Phi(\mathbf{z}_{UV}, \mathbf{z}_{\text{mesh}}),$$

where f_{θ} denotes the reconstruction network and Φ converts latent codes into posed 3D Gaussians.

In Sec. 3.1, we present the mask-based reconstruction model, centered on the dual-UV representation for robust alignment across varying input completeness, as shown in Fig. 2. Sec. 3.2 details the factorized synthetic data manifold curation pipeline that provides scalable and diverse supervision. Finally, Sec. 3.3 introduces the proxy mesh estimation framework for stable proxy mesh tracking. Refer to the supplementary for implementation and loss details.

3.1. Mask-based Reconstruction

Large reconstruction models [32, 86] map images to 3D by querying patch features with learnable tokens, which works for generic objects but entangles pose and identity for animatable humans. Because inputs vary greatly, from head-only to full-body, token correspondences become sensitive to framing and alignment, harming generalization. Moreover, these models must implicitly recover the canonical structure from posed images, even though the proxy mesh already provides the deformation field. This forces the decoder to relearn geometric mappings and wastes capacity.

We instead reconstruct through a geometry-aligned *Dual-UV representation* that deterministically maps image features into canonical UV space. This removes pose ambiguity, and lets the network focus solely on identity and appearance detail. The Dual-UV representation contains two complementary components.

Core-UV feature encoding. The Core-UV branch establishes a deterministic correspondence between image pixels and the canonical mesh surface. Using the UV layout of the

human mesh, we define a differentiable unparameterization

$$(u, v) = \mathcal{M}^{-1}(\mathbf{p}; M), \quad (1)$$

where each surface point \mathbf{p} on mesh M is uniquely mapped to its UV coordinate (u, v) . We uniformly sample surface points $\{\mathbf{p}_i\}_{i=1}^N$ on M and precompute their face indices and barycentric coordinates.

Given an input image I and calibrated camera Π , we follow previous works [71, 114], use a frozen Sapiens-1B encoder [40] to extract image features $\mathbf{F} = \mathcal{E}(I)$. We rasterize M under Π with back-face culling and z-buffering to determine visibility. For each visible point \mathbf{p}_i , it is projected to the image $\mathbf{x}_i = \Pi(\mathbf{p}_i)$, and its feature is gathered by:

$$\mathbf{f}_i = \mathcal{S}(\mathbf{F}, \mathbf{x}_i), \quad m_i \in \{0, 1\}, \quad (2)$$

where \mathcal{S} denotes differentiable bilinear sampling that interpolates local features from \mathbf{F} at subpixel coordinate \mathbf{x}_i . The sampled features are then scattered onto a regular UV grid $\tilde{\mathbf{U}} \in \mathbb{R}^{H_U \times W_U \times C}$:

$$\tilde{\mathbf{U}}(u, v) = \frac{\sum_i m_i k((u, v) - (u_i, v_i)) \mathbf{f}_i}{\sum_i m_i k((u, v) - (u_i, v_i)) + \varepsilon}, \quad (3)$$

where $k(\cdot)$ is a compact aggregation kernel (nearest-neighbor in practice) and ε ensures stability. This produces a canonical, geometry-aligned Core-UV feature map that provides a one-to-one, differentiable link between image observations and mesh-surface coordinates.

Shell-UV feature encoding. The human mesh M captures only the body surface and cannot represent volumetric details such as hair or loose garments. To encode these off-surface regions, we construct an auxiliary shell M^+ by offsetting each mesh vertex along its outward normal: $M^+ = \{\mathbf{p} + \delta \mathbf{n}(\mathbf{p}) \mid \mathbf{p} \in M\}$, where $\mathbf{n}(\mathbf{p})$ is the vertex normal and δ is a small offset distance. We rasterize

both M and M^+ under camera Π to obtain their visibility masks m_M and m_{M^+} . The *shell-only* region is defined as the visible area of S excluding the projection of M , $m_{\text{shell}} = m_{M^+} \cdot (1 - m_M)$, ensuring that only off-surface pixels are used for feature sampling.

For each visible point $\mathbf{p}_j \in M^+$ with $m_{\text{shell},j} = 1$, its projection $\mathbf{x}_j = \Pi(\mathbf{p}_j)$ queries the image feature map \mathbf{F} by differentiable bilinear sampling:

$$\mathbf{f}_j = \mathcal{S}(\mathbf{F}, \mathbf{x}_j). \quad (4)$$

The sampled features are transferred to their corresponding UV coordinates $(u_j, v_j) = \mathcal{M}^{-1}(\mathbf{p}_j)$ and aggregated on a coarse UV grid $\tilde{\mathbf{U}}_{\text{shell}} \in \mathbb{R}^{H'_U \times W'_U \times C}$ using the same kernel aggregation as in the Core-UV branch. Although the mapping from M^+ to UV space is approximate, it maintains local spatial coherence and provides a soft positional prior for encoding off-surface appearance.

Decoder Design. Core-UV and Shell-UV tokens are concatenated, processed by a shallow transformer stack, and unpatched to form the UV attributes. Separate heads predict Gaussian attributes in UV space, including color \mathbf{c} , opacity o , offset \mathbf{d} , and rotation \mathbf{r} and scale \mathbf{s} .

Discussion. Transformer-based avatar models [71, 114] typically employ large decoders with learnable queries, treating the pretrained encoder as a passive feature extractor and discarding the masked-autoencoding training asymmetry, where a strong encoder enables a lightweight decoder, as in Sapiens [40]. In contrast, we retain this asymmetry: projected image features fill only visible UV cells, leaving occluded regions blank, analogous to masked tokens. A compact transformer propagates information from visible to missing areas. This MAE-aligned design exploits pretrained reconstruction priors in geometry-aligned space, achieving high-quality avatars with far fewer decoder parameters than query-based approaches.

3.2. Dataset Curation

Training a single-image avatar reconstructor requires large-scale data that jointly cover geometric reliability and photorealistic diversity. Existing multi-view human datasets [34, 37, 58] are limited in identity and appearance due to costly studio capture. We therefore synthesize data from two complementary sources: a geometry-accurate *synthetic rendering branch* and a photorealistic *generative branch* (Fig. 3).

Synthetic Rendering Branch. We render multi-view human images with a parametric body model following [29]. Identity, pose, garment, and lighting are sampled procedurally, and each subject is rendered from multiple calibrated viewpoints under HDRI environments. This provides geometry-consistent supervision without manual annotation, forming the structural backbone of training data.

Generative Branch. While prior efforts [23, 114] fine-tune diffusion models for view-consistent humans, such constraints often degrade realism and diversity. We instead embrace a different philosophy: rather than forcing 2D generators to be multi-view consistent, we exploit their strengths, rich identity variation, natural appearance, and realistic motion, to populate a broad and controllable distribution of human imagery.

To this end, we define a *factorized data manifold* in which each sample is described by interpretable dimensions such as time of day, lighting, shot size, composition, clothing, hairstyle, role, region, and action. Combinations of these factors are first assembled into concise textual descriptions by GPT-5 [62], then refined by a large language model (Qwen2.5-14B-Instruct [78]) acting as a *realism regularizer*. This refinement step projects each prompt into a physically coherent, filmic space—resolving contradictory attributes and enriching it with cinematographic cues on framing, illumination, and tone. The refined prompts are passed to the text-to-video generator Wan2.2 [80] to produce short, temporally consistent human clips. From each clip, one representative frame is selected and complemented by side and back views synthesized through Qwen-Image-Edit [79]. Unlike prior works that assume perfect multi-view consistency, we treat these generated frames as weakly correlated views rather than ground-truth correspondences. During training, we impose a *directional cross-view consistency* that flows only from more reliable to less reliable views (e.g., side→back, front→back), avoiding cyclic constraints that can amplify identity drift or texture aliasing. This asymmetric design effectively stabilizes training while still encouraging view-aware coherence.

Discussion. Our design deliberately avoids fine-tuning generative models for 3D consistency, focusing instead on realism and diversity as complementary to the geometry-rich synthetic renders. Together, these two branches form a scalable corpus where geometry and photorealism are disentangled yet coherent: (i) the synthetic branch anchors geometric supervision, (ii) the generative branch expands appearance coverage within a factorized manifold, and (iii) the realism regularizer maintains filmic plausibility. This combination enables robust training and strong generalization to in-the-wild portraits. *Implementation details of the control factors, prompt templates, and LLM refinement commands are provided in the supplementary material.*

3.3. Proxy Mesh Estimation

A reliable proxy mesh is essential for canonical avatar reconstruction, yet many pretrained models can provide initial estimation, but each of them assumes its own cropped views and coordinate system. We therefore analyze the stability ranges of multiple estimators and build a unified tracking pipeline rather than relying on a single model.

We benchmark representative estimators across head-only, half-body, and full-body inputs. OSX performs well with half-body visibility; Multi-HMR delivers accurate estimates when the entire body is visible; EMICA remains stable for head-dominant inputs; HaMeR provides accurate hand articulation only when hands are visible. This yields an empirical map of each model’s reliable operating regime. Guided by this map, we design a hierarchical framework that activates and fuses outputs from multiple estimators according to detected visibility, then jointly refine via key-point reprojection and dense vertex alignment.

This tracker produces stable, anatomically coherent meshes for both real and generated images across all input types, from head-only portraits to full-body captures, and serves as a robust foundation for our reconstruction pipeline. Implementation details and further analyses are provided in the supplementary material.

4. Experiment

4.1. Implementation Details

We train on an upper-body–dominant synthetic dataset, while our data generation and training pipeline also flexibly accommodate full-body samples and head-only data. Our rendering pipeline generates 150K subjects assembled from curated 3D assets, each rendered from 12 upper-body–focused views. An additional 300K portrait video clips with talking or upper-body motion are synthesized, along with side and back views for a random frame. Data are split 19:1 for training and validation.

Our decoder has 8 self-attention layers and fewer than 0.1B parameters. Its outputs are unpatchified into 8×8 patches to form 512×512 Gaussian attribute maps (262K Gaussians). We train with AdamW [41] at a learning rate of 1×10^{-4} , using mixed precision and gradient clipping (norm 1.0). Training runs for three days on 4 NVIDIA A100 80G GPUs with a batch size of 8 per GPU, the overall training cost is *significantly lower* than LRM-based methods.

4.2. Experiment Setup

We compare with LHM, LHM-HF, IDOL, LAM, and GUAVA under head, upper-body, and full-body inputs.

LHM targets full-body reconstruction, encoding facial and body regions separately using DINOv2 [63] and Sapiens backbones for cross-attention between modalities. LHM-HF extends this design by training on half-body data augmented by random cropping from LHM’s large-scale in-the-wild video dataset. IDOL applies a large Transformer decoder along with a heavy CNN-based decoder to regress Gaussian attributes from learnable tokens. LAM simplifies LHM’s architecture, focusing on head modeling using both studio-captured [42] and in-the-wild data [96]. GUAVA specializes in upper-body reconstruction, featuring a dual-

branch Gaussian decoder followed by a screen-space CNN refinement [85] stage for improved fidelity.

For upper-body evaluation, we use 100 real clips from OpenHumanVid [48] and 200 synthetic clips; for head portraits, we sample 50 talking clips from RenderMe360 [64]; for full-body, we select 100 subjects from SHHQ [21]. We compare against the relevant baselines in each setting, using each method’s own tracking pipeline for preprocessing.

4.3. Comparison Results

Quantitative results are reported in Tab. 1 and qualitative comparisons in Fig. 4. For upper-body, our method surpasses LRM-based approaches (IDOL, LHM-HF) in texture fidelity and identity preservation. While GUAVA is competitive on visible regions, its strict requirement for visible hands causes unstable poses and artifacts under hand occlusions. In contrast, our method avoids any 2D refinement and remains robust across varying visibility conditions.

For head reconstruction, we outperform the head-specific LAM in identity preservation and additionally reconstruct regions below the shoulders that LAM cannot represent. In the full-body setting, our approach achieves performance comparable to dedicated single-image full-body methods, despite being trained almost exclusively on upper-body data and never seeing lower-body regions. This indicates strong generalization to unseen body parts.

As shown in Fig. 5, across all three settings our method produces novel views with consistent geometry and texture under diverse viewpoints and challenging poses.

4.4. Applications

Versatile Editing Our model exhibits strong generalization ability, allowing seamless integration with outputs from advanced image generation or editing models. As illustrated in Fig. 6, it can transform images synthesized by text-to-image or image-editing models into fully animatable 3D avatars, enabling flexible downstream editing and control.

Multiple Input Recent works [72] attempt to handle multi-view human images using computationally alternative attention [83]. In contrast, our method can naturally handle multi-view inputs by simply linearly blending the UV features from each image. As illustrated in Fig. 7, this simple strategy is sufficient to produce coherent reconstructions even in challenging multi-view scenarios.

4.5. Ablation Study

Model Design We ablate the decoder architecture, as summarized in Tab. 2 (a) and (d). Increasing the number of decoder layers leads to a consistent performance gain. In addition, introducing the shell token provides a clear boost, indicating that the extra token effectively enriches local surface modeling and, in turn, improves reconstruction quality.

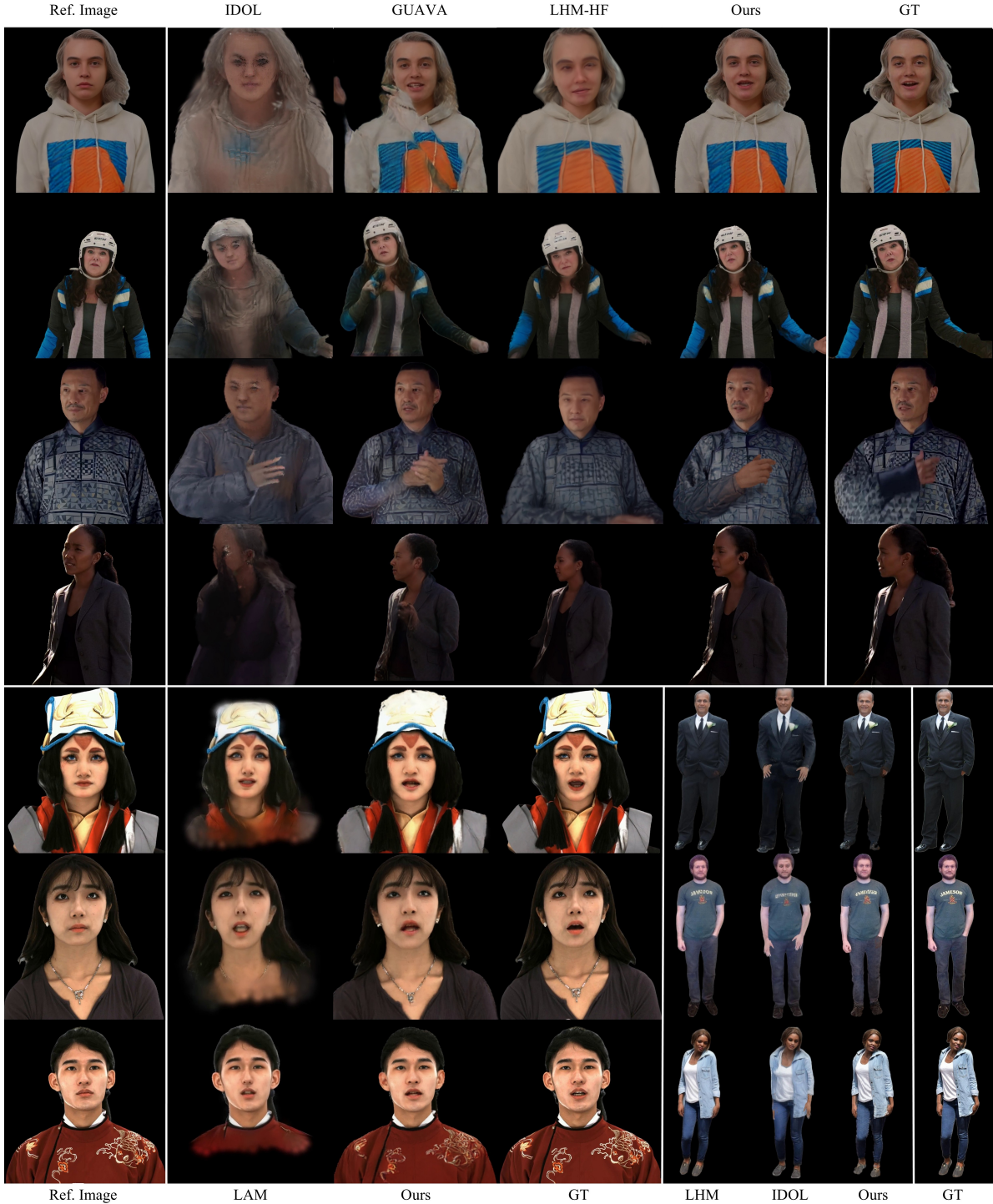


Figure 4. **Reenactment Results.** Our method is trained solely on *upper-body data only*, generalizes well to head and full-body inputs.

Table 1. Comparison of quantitative results with state-of-the-art methods.

	Upper-Wild			Upper-Wan				Full-Body				Head		
	PSNR↑	SSIM↑	LPIPS↓	PSNR↑	SSIM↑	LPIPS↓		PSNR↑	SSIM↑	LPIPS↓		PSNR↑	SSIM↑	LPIPS↓
Ours	21.09	0.8510	0.1426	20.38	0.7867	0.1635	Ours	24.53	0.8642	0.0916	Ours	19.04	0.8526	0.1613
GUAVA	20.59	0.7864	0.1957	20.24	0.7215	0.1940	IDOL	18.51	0.8753	0.1256	LAM†	17.19	0.7526	0.2207
LHM-HF	13.95	0.7835	0.3335	12.04	0.6664	0.3626	LHM	21.53	0.9151	0.0725	LAM	14.81	0.6789	0.2613
IDOL	12.93	0.7617	0.3465	10.35	0.5802	0.5132								

Note: **blue** and **lightblue** indicate the best and second-best results. † indicates non-facial parts are parsed out.



Figure 5. **Novel View Synthesis.** Our method generates multi-view human renderings from a single reference image, showing comparatively more consistent appearance, especially in the head and upper-body regions.



Figure 6. **Editing Results.** Our model supports various appearance edits from a single image, demonstrating its adaptability to diverse visual conditions.



Figure 7. **Multiple Input.** Our model is capable of taking multiple images as input, indicating its potential flexibility in leveraging multi-view information.

Dataset Scalability We also study the impact of training data type and scale. As shown in Tab. 2 (b) and (c), model performance improves steadily as the dataset grows, highlighting the benefit of larger and more diverse supervision.

When trained only on synthetic data *syn*, the model shows limited generalization. Using only generation data *gen* alleviates this issue, while *gen**, which contains only video-generated data without augmented images, performs worse. The best results are achieved when combining all data sources, suggesting that accurate 3D simulations com-

Table 2. Ablation study on model design and dataset scalability, evaluated on upper-body synthetic clips. **Blue** indicates the best results.

(a) Decoder depth				(b) Dataset scale				
blocks	PSNR \uparrow	SSIM \uparrow	LPIPS \downarrow	ratio	PSNR \uparrow	SSIM \uparrow	LPIPS \downarrow	
2	20.31	0.7846	0.1812	95%	20.38	0.7867	0.1635	
4	20.36	0.7862	0.1789	33%	20.33	0.7855	0.1801	
8	20.38	0.7867	0.1635	3%	20.25	0.7827	0.1888	
(c) Dataset type				(d) Shell token				
type	PSNR \uparrow	SSIM \uparrow	LPIPS \downarrow	PSNR \uparrow			SSIM \uparrow	LPIPS \downarrow
<i>full</i>	20.38	0.7867	0.1635	<i>w/ shell token</i>	20.38	0.7867	0.1635	
<i>syn</i>	19.57	0.7579	0.2418	<i>w/o shell token</i>	20.35	0.7845	0.1801	
<i>gen</i>	20.38	0.7861	0.1732					
<i>gen*</i>	20.34	0.7851	0.1794					

plemented by diverse 2D views are crucial for high-quality reconstruction.

5. Conclusion

We present a unified framework for reconstructing animatable 3D human avatars, spanning head-only, half-body, and full-body inputs within a single model. We train our model entirely on synthetic data yet generalizes well to in-the-wild portraits. Extensive experiments across head, upper-body, and full-body benchmarks demonstrate state-of-the-art or competitive performance, along with strong novel view synthesis and versatile applications such as reenactment, appearance editing, and multi-view fusion.

Despite these advances, our framework still has limitations. It relies on a proxy mesh that may fail under extreme or highly articulated poses, leading to noticeable reconstruction errors. And although our synthetic data manifold provides diverse identities and appearances, the views are still sparse, with limited side or rear perspectives, resulting in incomplete viewpoint coverage during training. Future work will explore weakly pose-dependent representations to mitigate these issues and further enhance robustness and generalization.

Acknowledgements

The authors would like to express their sincere gratitude to Paul McIlroy, Tadas Baltrusaitis, and Charlie Hewitt for generously providing the synthetic human rendering pipeline, which played a crucial role in this project. Additionally, we are deeply thankful to Ross Cutler’s team for their continuous support and insightful discussions, which greatly enhanced the quality of our work.

References

- [1] Rameen Abdal, Wang Yifan, Zifan Shi, Yinghao Xu, Ryan Po, Zhengfei Kuang, Qifeng Chen, Dit-Yan Yeung, and Gordon Wetzstein. Gaussian shell maps for efficient 3d human generation. In *CVPR*, 2024. 3
- [2] Sizhe An, Hongyi Xu, Yichun Shi, Guoxian Song, Umit Y. Ogras, and Linjie Luo. Panohead: Geometry-aware 3d full-head synthesis in 360deg. In *CVPR*, pages 20950–20959, 2023. 3
- [3] Fabien Baradel*, Matthieu Armando, Salma Galaoui, Romain Brégier, Philippe Weinzaepfel, Grégory Rogez, and Thomas Lucas*. Multi-hmr: Multi-person whole-body human mesh recovery in a single shot. In *ECCV*, 2024. 5
- [4] Jonathan T. Barron. A general and adaptive robust loss function, 2019. 7
- [5] Volker Blanz and Thomas Vetter. A morphable model for the synthesis of 3d faces. In *ACM TOG*, page 187–194, USA, 1999. ACM Press/Addison-Wesley Publishing Co. 3
- [6] Marcel C. Bühler, Ye Yuan, Xueting Li, Yangyi Huang, Koki Nagano, and Umar Iqbal. Dream, lift, animate: From single images to animatable gaussian avatars, 2025. 3
- [7] Hongrui Cai, Yuting Xiao, Xuan Wang, Jiafei Li, Yudong Guo, Yanbo Fan, Shenghua Gao, and Juyong Zhang. Hera: Hybrid explicit representation for ultra-realistic head avatars. In *CVPR*, 2025. 3
- [8] Chen Cao, Yanlin Weng, Shun Zhou, Yiyong Tong, and Kun Zhou. Facewarehouse: A 3d facial expression database for visual computing. *IEEE Transactions on Visualization and Computer Graphics*, 20(3):413–425, 2014. 2
- [9] Chen Cao, Hongzhi Wu, Yanlin Weng, Tianjia Shao, and Kun Zhou. Real-time facial animation with image-based dynamic avatars. *ACM TOG*, 35(4), 2016. 3
- [10] Eric Chan, Marco Monteiro, Petr Kellnhofer, Jiajun Wu, and Gordon Wetzstein. pi-gan: Periodic implicit generative adversarial networks for 3d-aware image synthesis. In *CVPR*, 2021. 3
- [11] Eric R. Chan, Connor Z. Lin, Matthew A. Chan, Koki Nagano, Boxiao Pan, Shalini De Mello, Orazio Gallo, Leonidas Guibas, Jonathan Tremblay, Sameh Khamis, Tero Karras, and Gordon Wetzstein. Efficient geometry-aware 3D generative adversarial networks. In *CVPR*, 2022. 3
- [12] Di Chang, Yichun Shi, Quankai Gao, Hongyi Xu, Jessica Fu, Guoxian Song, Qing Yan, Yizhe Zhu, Xiao Yang, and Mohammad Soleymani. Magicpose: Realistic human poses and facial expressions retargeting with identity-aware diffusion. In *ICML*, pages 6263–6285, 2024. 3
- [13] Jianchuan Chen, Jingchuan Hu, Gaige Wang, Zhonghua Jiang, Tiansong Zhou, Zhiwen Chen, and Chengfei Lv. Taoavatar: Real-time lifelike full-body talking avatars for augmented reality via 3d gaussian splatting. In *CVPR*, pages 10723–10734, 2025. 2
- [14] Wenyue Chen, Peng Li, Wangguandong Zheng, Chengfeng Zhao, Mengfei Li, Yaolong Zhu, Zhiyang Dou, Ronggang Wang, and Yuan Liu. Synchuman: Synchronizing 2d and 3d diffusion models for single-view human reconstruction. In *NeurIPS*, 2025. 3
- [15] Wei Cheng, Ruixiang Chen, Siming Fan, Wanqi Yin, Keyu Chen, Zhongang Cai, Jingbo Wang, Yang Gao, Zhengming Yu, Zhengyu Lin, Daxuan Ren, Lei Yang, Ziwei Liu, Chen Change Loy, Chen Qian, Wayne Wu, Dahua Lin, Bo Dai, and Kwan-Yee Lin. Dna-rendering: A diverse neural actor repository for high-fidelity human-centric rendering. In *ICCV*, pages 19982–19993, 2023. 2
- [16] Xuangeng Chu and Tatsuya Harada. Generalizable and animatable gaussian head avatar. In *The Thirty-eighth Annual Conference on Neural Information Processing Systems*, 2024. 7
- [17] Paul Debevec. The light stages and their applications to photoreal digital actors. *ACM TOG*, 2(4):1–6, 2012. 3
- [18] Zijian Dong, Xu Chen, Jinlong Yang, Michael J. Black, Otmar Hilliges, and Andreas Geiger. AG3D: Learning to generate 3D avatars from 2D image collections. In *ICCV*, 2023. 3
- [19] Patrick Esser, Robin Rombach, and Björn Ommer. Taming transformers for high-resolution image synthesis. In *Proceedings of the IEEE/CVF Conference on Computer Vision and Pattern Recognition (CVPR)*, pages 12873–12883, 2021. 3
- [20] Yao Feng, Vasileios Choutas, Timo Bolkart, Dimitrios Tzionas, and Michael J. Black. Collaborative regression of expressive bodies using moderation. In *International Conference on 3D Vision (3DV)*, 2021. 5
- [21] Jianglin Fu, Shikai Li, Yuming Jiang, Kwan-Yee Lin, Chen Qian, Chen-Change Loy, Wayne Wu, and Ziwei Liu. Stylegan-human: A data-centric odyssey of human generation. In *ECCV*, pages 729–747, 2022. 3, 6
- [22] Xuan Gao, Haiyao Xiao, Chenglai Zhong, Shimin Hu, Yudong Guo, and Juyong Zhang. Portrait video editing empowered by multimodal generative priors. In *SIGGRAPH Asia Conference Proceedings*, 2024. 3
- [23] Xuan Gao, Jingtao Zhou, Dongyu Liu, Yuqi Zhou, and Juyong Zhang. Controlling avatar diffusion with learnable gaussian embedding. In *Proceedings of SIGGRAPH Asia 2025*, 2025. 3, 5
- [24] Jiazhi Guan, Quanwei Yang, Kaisiyuan Wang, Hang Zhou, Shengyi He, Zhiliang Xu, Haocheng Feng, Errui Ding, Jingdong Wang, Hongtao Xie, Youjian Zhao, and Ziwei Liu. Talk-act: Enhance textural-awareness for 2d speaking avatar reenactment with diffusion model. In *SIGGRAPH Asia 2024 Conference Papers*, 2024. 3
- [25] Chen Guo, Tianjian Jiang, Xu Chen, Jie Song, and Otmar Hilliges. Vid2avatar: 3d avatar reconstruction from videos in the wild via self-supervised scene decomposition. In *CVPR*, 2023. 3

- [26] Chen Guo, Zhuo Su, Jian Wang, Shuang Li, Xu Chang, Zhaohu Li, Yang Zhao, Guidong Wang, and Ruqi Huang. Sega: Drivable 3d gaussian head avatar from a single image, 2025. 3
- [27] Sang-Hun Han, Min-Gyu Park, Ju Hong Yoon, Ju-Mi Kang, Young-Jae Park, and Hae-Gon Jeon. High-fidelity 3d human digitization from single 2k resolution images. In *CVPR*, 2023. 2
- [28] Yisheng He, Xiaodong Gu, Xiaodan Ye, Chao Xu, Zhengyi Zhao, Yuan Dong, Weihao Yuan, Zilong Dong, and Liefeng Bo. Lam: Large avatar model for one-shot animatable gaussian head. In *Proceedings of SIGGRAPH*, pages 1–13, 2025. 1, 3
- [29] Charlie Hewitt, Fatemeh Saleh, Sadegh Aliakbarian, Lohit Petikam, Shideh Rezaeifar, Louis Florentin, Zafirah Hosenie, Thomas J Cashman, Julien Valentin, Darren Cosker, and Tadas Baltrušaitis. Look ma, no markers: holistic performance capture without the hassle. *ACM TOG*, 43(6), 2024. 3, 5, 2
- [30] Fangzhou Hong, Zhaoxi Chen, Yushi Lan, Liang Pan, and Ziwei Liu. Eva3d: Compositional 3d human generation from 2d image collections. *ICLR*, 2022. 3
- [31] Yang Hong, Bo Peng, Haiyao Xiao, Ligang Liu, and Juyong Zhang. Headnerf: A real-time nerf-based parametric head model. In *CVPR*, 2022. 3
- [32] Yicong Hong, Kai Zhang, Jiuxiang Gu, Sai Bi, Yang Zhou, Difan Liu, Feng Liu, Kalyan Sunkavalli, Trung Bui, and Hao Tan. Lrm: Large reconstruction model for single image to 3d. In *ICLR*, 2024. 1, 3, 4
- [33] Yangyi Huang, Ye Yuan, Xueting Li, Jan Kautz, and Umar Iqbal. Adahuman: Animatable detailed 3d human generation with compositional multiview diffusion. In *Proceedings of the IEEE/CVF International Conference on Computer Vision (ICCV)*, pages 13533–13543, 2025. 3
- [34] Mustafa Işık, Martin Rünz, Markos Georgopoulos, Taras Khakhulin, Jonathan Starck, Lourdes Agapito, and Matthias Nießner. Humanrf: High-fidelity neural radiance fields for humans in motion. *ACM TOG*, 42(4):1–12, 2023. 2, 5
- [35] Yasamin Jafarian and Hyun Soo Park. Learning high fidelity depths of dressed humans by watching social media dance videos. In *CVPR*, pages 12753–12762, 2021. 3
- [36] Yudong Jin, Sida Peng, Xuan Wang, Tao Xie, Zhen Xu, Yifan Yang, Yujun Shen, Hujun Bao, and Xiaowei Zhou. Difuman4d: 4d consistent human view synthesis from sparse-view videos with spatio-temporal diffusion models. In *ICCV*, 2025. 3
- [37] Yash Kant, Ethan Weber, Jin Kyu Kim, Rawal Khirodkar, Su Zhaoen, Julieta Martinez, Igor Gilitschenski, Shunsuke Saito, and Timur Bagautdinov. Pippo: High-resolution multi-view humans from a single image. In *CVPR*, 2025. 3, 5
- [38] Tero Karras, Samuli Laine, and Timo Aila. A style-based generator architecture for generative adversarial networks. *IEEE Transactions on Pattern Analysis and Machine Intelligence*, 43(12):4217–4228, 2021. 3
- [39] Bernhard Kerbl, Georgios Kopanas, Thomas Leimkühler, and George Drettakis. 3d gaussian splatting for real-time radiance field rendering. *ACM TOG*, 42(4), 2023. 3
- [40] Rawal Khirodkar, Timur Bagautdinov, Julieta Martinez, Zhaoen Su, Austin James, Peter Selednik, Stuart Anderson, and Shunsuke Saito. Sapiens: Foundation for human vision models. In *ECCV*, 2024. 4, 5
- [41] Diederik P. Kingma and Jimmy Ba. Adam: A method for stochastic optimization, 2017. 6, 7
- [42] Tobias Kirschstein, Shenhan Qian, Simon Giebenhain, Tim Walter, and Matthias Nießner. Nersemble: Multi-view radiance field reconstruction of human heads. *ACM TOG*, 2023. 2, 6
- [43] Tobias Kirschstein, Simon Giebenhain, Jiapeng Tang, Markos Georgopoulos, and Matthias Nießner. GGHead: Fast and Generalizable 3D Gaussian Heads. In *SIGGRAPH Asia Conference Papers*, 2024. 3
- [44] Nikos Kolotouros, Thiemo Alldieck, Andrei Zanfir, Eduard Bazavan, Mihai Fieraru, and Cristian Sminchisescu. Dreamhuman: Animatable 3d avatars from text. *NeurIPS*, 36:10516–10529, 2023. 3
- [45] Jason Lawrence, Danb Goldman, Supreeth Achar, Gregory Major Blascovich, Joseph G. Desloge, Tommy Fortes, Eric M. Gomez, Sascha Häberling, Hugues Hoppe, Andy Huibers, Claude Knaus, Brian Kuschak, Ricardo Martin-Brualla, Harris Nover, Andrew Ian Russell, Steven M. Seitz, and Kevin Tong. Project starline: a high-fidelity telepresence system. *ACM TOG*, 40(6), 2021. 3
- [46] Heyuan Li, Ce Chen, Tianhao Shi, Yuda Qiu, Sizhe An, Guanying Chen, and Xiaoguang Han. Spherehead: Stable 3d full-head synthesis with spherical tri-plane representation. In *ECCV*, 2024. 3
- [47] Heyuan Li, Kenkun Liu, Lingteng Qiu, Qi Zuo, Keru Zheng, Zilong Dong, and Xiaoguang Han. Hyplanehead: Rethinking tri-plane-like representations in full-head image synthesis. In *NeurIPS*, 2025. Poster. 3
- [48] Hui Li, Mingwang Xu, Yun Zhan, Shan Mu, Jiaye Li, Kaihui Cheng, Yuxuan Chen, Tan Chen, Mao Ye, Jingdong Wang, et al. Openhumanvid: A large-scale high-quality dataset for enhancing human-centric video generation. In *CVPR*, 2025. 3, 6
- [49] Junxuan Li, Chen Cao, Gabriel Schwartz, Rawal Khirodkar, Christian Richardt, Tomas Simon, Yaser Sheikh, and Shunsuke Saito. Uravatar: Universal relightable gaussian codec avatars. In *SIGGRAPH Conference Papers*, 2024. 3
- [50] Peng Li, Wangguandong Zheng, Yuan Liu, Tao Yu, Yangguang Li, Xingqun Qi, Mengfei Li, Xiaowei Chi, Siyu Xia, Wei Xue, et al. Pshuman: Photorealistic single-view human reconstruction using cross-scale diffusion. In *CVPR*, 2025. 3
- [51] Tianye Li, Timo Bolkart, Michael J. Black, Hao Li, and Javier Romero. Learning a model of facial shape and expression from 4D scans. *ACM TOG*, 36(6):194:1–194:17, 2017. 1
- [52] Zhe Li, Zerong Zheng, Lizhen Wang, and Yebin Liu. Animatable gaussians: Learning pose-dependent gaussian maps for high-fidelity human avatar modeling. In *Proceed-*

- ings of the *IEEE/CVF conference on computer vision and pattern recognition*, pages 19711–19722, 2024. 3
- [53] Gaojie Lin, Jianwen Jiang, Chao Liang, Tianyun Zhong, Jiaqi Yang, Zerong Zheng, and Yanbo Zheng. Cyberhost: A one-stage diffusion framework for audio-driven talking body generation. In *ICLR*, 2025. 3
- [54] Jing Lin, Ailing Zeng, Haoqian Wang, Lei Zhang, and Yu Li. One-stage 3d whole-body mesh recovery with component aware transformer. In *CVPR*, pages 21159–21168, 2023. 5
- [55] Haiyang Liu, Xingchao Yang, Tomoya Akiyama, Yuantian Huang, Qiaoge Li, Shigeru Kuriyama, and Takafumi Takeuchi. Tango: Co-speech gesture video reenactment with hierarchical audio motion embedding and diffusion interpolation. In *ICLR*, 2025. 3
- [56] Xian Liu, Xiaohang Zhan, Jiayang Tang, Ying Shan, Gang Zeng, Dahua Lin, Xihui Liu, and Ziwei Liu. Humangaussian: Text-driven 3d human generation with gaussian splatting. In *CVPR*, 2024. 3
- [57] Yixing Lu, Junting Dong, Youngjoong Kwon, Qin Zhao, Bo Dai, and Fernando De la Torre. Gas: Generative avatar synthesis from a single image. In *ICCV*, 2025. 3
- [58] Julieta Martinez, Emily Kim, Javier Romero, et al. Codec Avatar Studio: Paired Human Captures for Complete, Driveable, and Generalizable Avatars. *NeurIPS*, 2024. 2, 5
- [59] Ben Mildenhall, Pratul P. Srinivasan, Matthew Tancik, Jonathan T. Barron, Ravi Ramamoorthi, and Ren Ng. Nerf: Representing scenes as neural radiance fields for view synthesis. In *ECCV*, 2020. 3
- [60] Gyeongsik Moon, Takaaki Shiratori, and Shunsuke Saito. Expressive whole-body 3D gaussian avatar. In *ECCV*, 2024. 3
- [61] Jorge Nocedal and Stephen J. Wright. *Numerical Optimization*. Springer, New York, NY, USA, second edition, 2006. 2
- [62] OpenAI. Introducing gpt-5, 2025. Blog post. 5
- [63] Maxime Oquab, Timothée Darcet, Theo Moutakanni, Huy V. Vo, Marc Szafraniec, Vasil Khalidov, Pierre Fernandez, Daniel Haziza, Francisco Massa, Alaaeldin El-Nouby, Russell Howes, Po-Yao Huang, Hu Xu, Vasu Sharma, Shang-Wen Li, Wojciech Galuba, Mike Rabbat, Mido Assran, Nicolas Ballas, Gabriel Synnaeve, Ishan Misra, Herve Jegou, Julien Mairal, Patrick Labatut, Armand Joulin, and Piotr Bojanowski. Dinov2: Learning robust visual features without supervision, 2023. 6
- [64] Dongwei Pan, Long Zhuo, Jingtan Piao, Huiwen Luo, Wei Cheng, Yuxin Wang, Siming Fan, Shengqi Liu, Lei Yang, Bo Dai, Ziwei Liu, Chen Change Loy, Chen Qian, Wayne Wu, Dahua Lin, and Kwan-Yee Lin. Renderme-360: Large digital asset library and benchmark towards high-fidelity head avatars. In *Thirty-seventh Conference on Neural Information Processing Systems Datasets and Benchmarks Track*, 2023. 6
- [65] Panwang Pan, Zhuo Su, Chenguo Lin, Zhen Fan, Yongjie Zhang, Zeming Li, Tingting Shen, Yadong Mu, and Yebin Liu. Humansplat: Generalizable single-image human gaussian splatting with structure priors. In *NeurIPS*, 2024. 3
- [66] Georgios Pavlakos, Vasileios Choutas, Nima Ghorbani, Timo Bolkart, Ahmed A. A. Osman, Dimitrios Tzionas, and Michael J. Black. Expressive body capture: 3D hands, face, and body from a single image. In *CVPR*, pages 10975–10985, 2019. 1
- [67] Georgios Pavlakos, Dandan Shan, Ilija Radosavovic, Angjoo Kanazawa, David Fouhey, and Jitendra Malik. Reconstructing hands in 3D with transformers. In *CVPR*, 2024. 7
- [68] Sida Peng, Yuanqing Zhang, Yinghao Xu, Qianqian Wang, Qing Shuai, Hujun Bao, and Xiaowei Zhou. Neural body: Implicit neural representations with structured latent codes for novel view synthesis of dynamic humans. In *CVPR*, 2021. 3
- [69] Ben Poole, Ajay Jain, Jonathan T. Barron, and Ben Mildenhall. Dreamfusion: Text-to-3d using 2d diffusion. In *ICLR*, 2023. 3
- [70] Shenhan Qian, Tobias Kirschstein, Liam Schoneveld, Davide Davoli, Simon Giebenhain, and Matthias Nießner. Gaussianavatars: Photorealistic head avatars with rigged 3d gaussians. In *CVPR*, 2023. 3
- [71] Lingteng Qiu, Xiaodong Gu, Peihao Li, Qi Zuo, Weichao Shen, Junfei Zhang, Kejie Qiu, Weihao Yuan, Guanying Chen, Zilong Dong, and Liefeng Bo. Lhm: Large animatable human reconstruction model from a single image in seconds. In *ICCV*, 2025. 1, 3, 4, 5
- [72] Lingteng Qiu, Peihao Li, Qi Zuo, Xiaodong Gu, Yuan Dong, Weihao Yuan, Siyu Zhu, Xiaoguang Han, Guanying Chen, and Zilong Dong. Pf-lhm: 3d animatable avatar reconstruction from pose-free articulated human images, 2025. 6
- [73] Lingteng Qiu, Shenhao Zhu, Qi Zuo, Xiaodong Gu, Yuan Dong, Junfei Zhang, Chao Xu, Zhe Li, Weihao Yuan, Liefeng Bo, et al. Anigs: Animatable gaussian avatar from a single image with inconsistent gaussian reconstruction. In *CVPR*, 2025. 3
- [74] Robin Rombach, Andreas Blattmann, Dominik Lorenz, Patrick Esser, and Björn Ommer. High-resolution image synthesis with latent diffusion models. In *CVPR*, pages 10684–10695, 2022. 3
- [75] Shunsuke Saito, Zeng Huang, Ryota Natsume, Shigeo Morishima, Angjoo Kanazawa, and Hao Li. Pifu: Pixel-aligned implicit function for high-resolution clothed human digitization. In *ICCV*, pages 2304–2313, 2019. 3
- [76] Shunsuke Saito, Gabriel Schwartz, Tomas Simon, Junxuan Li, and Giljoo Nam. Relightable gaussian codec avatars. In *CVPR*, 2024. 3
- [77] Jiayang Tang, Jiawei Ren, Hang Zhou, Ziwei Liu, and Gang Zeng. Dreamgaussian: Generative gaussian splatting for efficient 3d content creation. In *ICLR*, 2024. 3
- [78] Qwen Team. Qwen2.5 technical report, 2025. 5, 4
- [79] Qwen-Image Team. Qwen-image technical report, 2025. 5, 4
- [80] Wan Team. Wan: Open and advanced large-scale video generative models, 2025. 5, 4
- [81] Timo Teufel, Xilong Zhou, Umar Iqbal, Pramod Rao, Pulkit Gera, Jan Kautz, Vladislav Golyanik, and Christian

- Theobalt. Humanolat: A large-scale dataset for full-body human relighting and novel-view synthesis. In *ICCV*, 2025. 2
- [82] Hanzhang Tu, Ruizhi Shao, Xue Dong, Shunyuang Zheng, Hao Zhang, Lili Chen, Meili Wang, Wenyu Li, Siyan Ma, Shengping Zhang, Boyao Zhou, and Yebin Liu. Telealoha: A telepresence system with low-budget and high-authenticity using sparse rgb cameras. In *ACM SIGGRAPH 2024 Conference Papers*, New York, NY, USA, 2024. Association for Computing Machinery. 3
- [83] Jianyuan Wang, Minghao Chen, Nikita Karaev, Andrea Vedaldi, Christian Rupprecht, and David Novotny. Vggt: Visual geometry grounded transformer. In *CVPR*, 2025. 6
- [84] Lizhen Wang, Zhiyua Chen, Tao Yu, Chenguang Ma, Liang Li, and Yebin Liu. Faceverse: a fine-grained and detail-controllable 3d face morphable model from a hybrid dataset. In *CVPR*, 2022. 2
- [85] Lizhen Wang, Xiaochen Zhao, Jingxiang Sun, Yuxiang Zhang, Hongwen Zhang, Tao Yu, and Yebin Liu. Styleavatar: Real-time photo-realistic portrait avatar from a single video. In *SIGGRAPH Conference Proceedings*, 2023. 6
- [86] Peng Wang, Hao Tan, Sai Bi, Yinghao Xu, Fujun Luan, Kalyan Sunkavalli, Wenping Wang, Zexiang Xu, and Kai Zhang. Pflrm: Pose-free large reconstruction model for joint pose and shape prediction. In *ICLR*, 2024. 3, 4
- [87] Shaofei Wang, Tomas Simon, Igor Santesteban, Timur Bagautdinov, Junxuan Li, Vasu Agrawal, Fabian Prada, Shou-I Yu, Pace Nalbani, Matt Gramlich, Roman Lubachersky, Chenglei Wu, Javier Romero, Jason Saragih, Michael Zollhoefer, Andreas Geiger, Siyu Tang, and Shunsuke Saito. Relightable full-body gaussian codec avatars. In *SIGGRAPH Conference Papers*, 2025. 3
- [88] Tengfei Wang, Bo Zhang, Ting Zhang, Shuyang Gu, Jianmin Bao, Tadas Baltrusaitis, Jingjing Shen, Dong Chen, Fang Wen, Qifeng Chen, and Baining Guo. Rodin: A generative model for sculpting 3d digital avatars using diffusion. In *CVPR*, pages 4563–4573, 2023. 3
- [89] Yanwen Wang, Yiyu Zhuang, Jiawei Zhang, Li Wang, Yifei Zeng, Xun Cao, Xinxin Zuo, and Hao Zhu. Tera: Rethinking text-guided realistic 3d avatar generation. In *ICCV*, pages 10686–10697, 2025. 3
- [90] Yue Wu, Sicheng Xu, Jianfeng Xiang, Fangyun Wei, Qifeng Chen, Jiaolong Yang, and Xin Tong. Aniportraitgan: Animatable 3d portrait generation from 2d image collections. In *SIGGRAPH Asia Conference Proceedings*, 2023. 3
- [91] Yiqian Wu, Hao Xu, Xiangjun Tang, Xien Chen, Siyu Tang, Zhebin Zhang, Chen Li, and Xiaogang Jin. Portrait3d: Text-guided high-quality 3d portrait generation using pyramid representation and gans prior. *ACM TOG*, 43(4), 2024.
- [92] Yiqian Wu, Malte Prinzler, Xiaogang Jin, and Siyu Tang. Text-based animatable 3d avatars with morphable model alignment. In *SIGGRAPH Conference Proceedings*. Association for Computing Machinery, 2025.
- [93] Yiqian Wu, Hao Xu, Xiangjun Tang, Yue Shangguan, Hongbo Fu, and Xiaogang Jin. 3dportraitgan: Learning one-quarter headshot 3d gans from a single-view portrait dataset with diverse body poses. *IEEE Transactions on Circuits and Systems for Video Technology*, pages 1–1, 2025. 3
- [94] Jun Xiang, Xuan Gao, Yudong Guo, and Juyong Zhang. Flashavatar: High-fidelity head avatar with efficient gaussian embedding. In *CVPR*, 2024. 3
- [95] Jun Xiang, Yudong Guo, Leipeng Hu, Boyang Guo, Yancheng Yuan, and Juyong Zhang. Expressive talking human from single-image with imperfect priors. In *ICCV*, 2025. 3
- [96] Liangbin Xie, Xintao Wang, Honglun Zhang, Chao Dong, and Ying Shan. Vfhq: A high-quality dataset and benchmark for video face super-resolution. In *CVPRW*, 2022. 3, 6
- [97] Zhangyang Xiong, Chenghong Li, Kenkun Liu, Hongjie Liao, Jianqiao Hu, Junyi Zhu, Shuliang Ning, Lingteng Qiu, Chongjie Wang, Shijie Wang, et al. Mvhumannet: A large-scale dataset of multi-view daily dressing human captures. In *CVPR*, pages 19801–19811, 2024. 2
- [98] Yuliang Xiu, Jinlong Yang, Dimitrios Tzionas, and Michael J. Black. ICON: Implicit Clothed humans Obtained from Normals. In *CVPR*, pages 13296–13306, 2022. 3
- [99] Yuliang Xiu, Jinlong Yang, Xu Cao, Dimitrios Tzionas, and Michael J. Black. ECON: Explicit Clothed humans Optimized via Normal integration. In *CVPR*, 2023. 3
- [100] Yuelang Xu, Benwang Chen, Zhe Li, Hongwen Zhang, Lizhen Wang, Zerong Zheng, and Yebin Liu. Gaussian head avatar: Ultra high-fidelity head avatar via dynamic gaussians. In *CVPR*, pages 1931–1941, 2024. 3
- [101] Zhen Xu, Sida Peng, Chen Geng, Linzhan Mou, Zihan Yan, Jiaming Sun, Hujun Bao, and Xiaowei Zhou. Relightable and animatable neural avatar from sparse-view video. In *CVPR*, 2024. 3
- [102] Haotian Yang, Hao Zhu, Yanru Wang, Mingkai Huang, Qiu Shen, Ruigang Yang, and Xun Cao. Facescape: a large-scale high quality 3d face dataset and detailed riggable 3d face prediction. In *CVPR*, 2020. 2
- [103] Zhitao Yang, Zhongang Cai, Haiyi Mei, Shuai Liu, Zhaoxi Chen, Weiye Xiao, Yukun Wei, Zhongfei Qing, Chen Wei, Bo Dai, Wayne Wu, Chen Qian, Dahua Lin, Ziwei Liu, and Lei Yang. Synbody: Synthetic dataset with layered human models for 3d human perception and modeling. In *ICCV*, pages 20282–20292, 2023. 3
- [104] Houteng Yu, Hao Zhu, and Xun Cao. Realityavatar: Comprehensive head avatar generation with 360° rendering. In *2025 IEEE International Conference on Multimedia and Expo (ICME)*, pages 1–6, 2025. 3
- [105] Tao Yu, Zerong Zheng, Kaiwen Guo, Pengpeng Liu, Qionghai Dai, and Yebin Liu. Function4d: Real-time human volumetric capture from very sparse consumer rgbd sensors. In *CVPR*, 2021. 2
- [106] Zhengming Yu, Tianye Li, Jingxiang Sun, Omer Shapira, Seonwook Park, Michael Stengel, Matthew Chan, Xin Li, Wenping Wang, Koki Nagano, and Shalini De Mello. GAIA: Generative animatable interactive avatars with expression-conditioned gaussians. In *SIGGRAPH Asia Conference Papers*, 2025. 3

- [107] Dongbin Zhang, Yunfei Liu, Lijian Lin, Ye Zhu, Yang Li, Minghan Qin, Yu Li, and Haoqian Wang. Guava: Generalizable upper body 3d gaussian avatar. In *ICCV*, 2025. 3
- [108] Jiawei Zhang, Zijian Wu, Zhiyang Liang, Yicheng Gong, Dongfang Hu, Yao Yao, Xun Cao, and Hao Zhu. Fate: Full-head gaussian avatar with textural editing from monocular video. In *Proceedings of the Computer Vision and Pattern Recognition Conference*, pages 5535–5545, 2025. 3
- [109] Xuanmeng Zhang, Jianfeng Zhang, Chacko Rohan, Hongyi Xu, Guoxian Song, Yi Yang, and Jiashi Feng. Getavatar: Generative textured meshes for animatable human avatars. In *ICCV*, 2023. 3
- [110] Zechuan Zhang, Zongxin Yang, and Yi Yang. Sifu: Side-view conditioned implicit function for real-world usable clothed human reconstruction. In *CVPR*, pages 9936–9947, 2024. 3
- [111] Yufeng Zheng, Victoria Fernández Abrevaya, Marcel C. Bühler, Xu Chen, Michael J. Black, and Otmar Hilliges. I M Avatar: Implicit morphable head avatars from videos. In *CVPR*, 2022. 3
- [112] Yufeng Zheng, Wang Yifan, Gordon Wetzstein, Michael J. Black, and Otmar Hilliges. Pointavatar: Deformable point-based head avatars from videos. In *CVPR*, 2023. 3
- [113] Zhenglin Zhou, Fan Ma, Hehe Fan, Zongxin Yang, and Yi Yang. Headstudio: Text to animatable head avatars with 3d gaussian splatting. In *ECCV*, 2024. 3
- [114] Yiyu Zhuang, Jiayi Lv, Hao Wen, Qing Shuai, Ailing Zeng, Hao Zhu, Shifeng Chen, Yujiu Yang, Xun Cao, and Wei Liu. Idol: Instant photorealistic 3d human creation from a single image. In *CVPR*, pages 26308–26319, 2025. 3, 4, 5

Bringing Your Portrait to 3D Presence

Supplementary Material



Figure 8. A conceptual illustration of *Bringing Your Portrait to 3D Presence*. Our pipeline transforms everyday portrait images into fully controllable 3D avatars that can be animated via a tracked proxy mesh. The model is trained entirely on a hybrid synthetic corpus combining rendered and generative sources. Thanks to our dual-UV representation, the system robustly handles inputs of varying completeness—ranging from head-only to half-body or full-body portraits—within a single unified framework.

We provide the model design and training procedure in Sec. A, the details of our dataset curation in Sec. B, the proxy-mesh estimation pipeline in Sec. C. Additional qualitative results are shown in the supplementary videos.

A. Model Details

A.1. Model Design

After scattering UV features, we add separate learnable positional embeddings for different UV branches. For the *core-UV* branch, we initialize the positional embedding in UV coordinates. Concretely, we rasterize the vertices of the canonical-space template mesh into the UV plane and obtain a position map shown in Fig. 9, with the same spatial resolution as the UV feature map. We then apply an L -frequency sinusoidal encoding to each UV coordinate, with $L = 8$, and pass the encoded features through a linear layer to project them to the Sapiens feature dimension. For the *shell-UV* branch, we initialize the learnable tokens with Gaussian noise.

The UV features with positional embeddings are linearly projected to 1024 and processed by 8 self-attention blocks

with 16 attention heads each, to model interactions among tokens. We then perform unpatchify with patch size 8 to form Gaussian attribute maps. For different Gaussian attributes, we use separate decoder heads, each implemented as a two-layer MLP with 256 hidden dimension and SiLU activation. We uniformly sample from the decoded Gaussian attribute maps and slightly retopologize the UV layout so that the utilization of tokens is as high as possible.

During training, we randomly mask from 0% to 50% of the scattered UV features to improve robustness. At test time, we use the input image mask to filter out points that fall outside the masked region due to mesh misalignment. This simple trick effectively prevents artifacts caused by proxy-mesh misalignment.

A.2. Loss function

Given a reference–target pair, we predict canonical Gaussian attributes from the reference, rig them to the target mesh, and render both views. The total objective combines reconstruction and regularization terms:

$$\mathcal{L} = \mathcal{L}_{\text{rec}} + \mathcal{L}_{\text{regu}}. \quad (5)$$

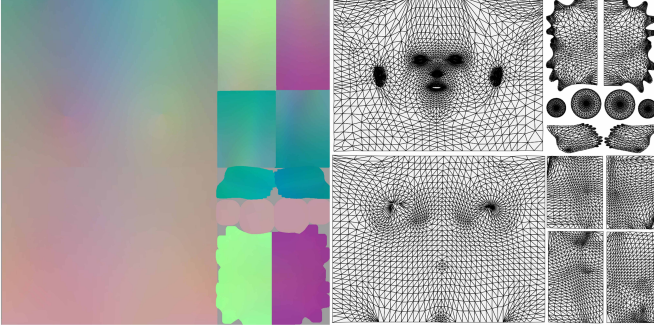


Figure 9. **UV Topology Visualization and Position Map.** We visualize the modified UV topology and the corresponding position map used for sinusoidal encoding.

Reconstruction loss. For each view $v \in \{\text{ref}, \text{tgt}\}$, we supervise image fidelity using pixel and perceptual losses:

$$\mathcal{L}_{\text{rec}}^{(v)} = \lambda_{L1} \left\| \hat{I}^{(v)} - I^{(v)} \right\|_1 + \lambda_{\text{LPIPS}} \mathcal{L}_{\text{LPIPS}} \left(\hat{I}^{(v)}, I^{(v)} \right), \quad (6)$$

with $\lambda_{L1} = 1.0$ and $\lambda_{\text{LPIPS}} = 0.5$. The reconstruction loss sums over both views:

$$\mathcal{L}_{\text{rec}} = \mathcal{L}_{\text{rec}}^{\text{ref}} + \mathcal{L}_{\text{rec}}^{\text{tgt}}. \quad (7)$$

Geometry regularization. We constrain Gaussian geometry parameters to ensure stability. Offsets are penalized to prevent drift:

$$\mathcal{L}_o = \|\mathbf{d}\|_2, \quad (8)$$

and scales $\mathbf{s} = [s_x, s_y, s_z]$ are regularized for compactness and isotropy:

$$\mathcal{L}_s = \sum_{i \in \{x, y, z\}} s_i, \quad (9)$$

$$\mathcal{L}_r = \max \left(\frac{\max(\mathbf{s})}{\min(\mathbf{s})} - r, 0 \right), \quad (10)$$

where $r=9$. The geometry regularization term is

$$\mathcal{L}_{\text{geo}} = \lambda_o \mathcal{L}_o + \lambda_s \mathcal{L}_s + \lambda_r \mathcal{L}_r. \quad (11)$$

Texture regularization. We further regularize Gaussian appearance to avoid implausible color and opacity distributions. A hand-consistency loss aligns hand and facial color statistics by matching each hand patch \mathbf{P}_i^h to its nearest facial patch \mathbf{P}_j^f (gradient detached):

$$\mathcal{L}_h = \sum_i \min_j \|\mathbf{P}_i^h - \mathbf{P}_j^f\|_2. \quad (12)$$

In addition, we impose a patch-level regularization on the opacity. For each Gaussian opacity map, we divide it into patches and enforce that the average opacity in each

patch is close to a target value α_{ref} , which we set as 0.8. The opacity loss for each patch is defined as:

$$\mathcal{L}_\alpha = -\frac{1}{N} \sum_{k=1}^N (\alpha_{\text{ref}} \cdot \log(\mu_k) + (1 - \alpha_{\text{ref}}) \cdot \log(1 - \mu_k)), \quad (13)$$

where μ_k is the mean opacity of the k -th patch, and N is the number of patches.

The texture regularization term is

$$\mathcal{L}_{\text{tex}} = \lambda_h \mathcal{L}_h + \lambda_\alpha \mathcal{L}_\alpha. \quad (14)$$

Finally, the total regularization is

$$\mathcal{L}_{\text{regu}} = \mathcal{L}_{\text{geo}} + \mathcal{L}_{\text{tex}}, \quad (15)$$

with $(\lambda_o, \lambda_s, \lambda_r, \lambda_h, \lambda_\alpha) = (1.0, 0.1, 1.0, 0.1, 0.1)$ in all experiments.

B. Dataset Details

B.1. Synthetic Rendering Branch

Our synthetic rendering pipeline begins by sampling shape and pose parameters from the SOMA parametric human model [29]. Given the sampled body and pose coefficients, we apply texture, hair and clothing assets upon posed mesh. And further sample a HDR image to set up environment lighting. The full scene is rendered using the Cycles rendering engine. For camera configuration, we adaptively determine the look-at point based on the posed subject rather than using a fixed center. Let v_{min} and v_{max} denote the minimum and maximum vertex positions in world space along the vertical axis, and let \mathbf{p}_{pel} and \mathbf{p}_{head} be the pelvis and head joint locations, respectively. We define the horizontal look-at target as

$$\mathbf{t}_{xy} = \frac{\mathbf{p}_{\text{pel}} + \mathbf{p}_{\text{head}}}{2}, \quad (16)$$

and the vertical target coordinates as

$$t_z = v_{\text{min}} + \lambda \cdot (v_{\text{max}} - v_{\text{min}}), \quad \lambda = 0.75. \quad (17)$$

Thus, the final camera look-at position is $\mathbf{t} = (\mathbf{t}_{xy}, t_z)$, which biases the view toward the upper-body and yields perceptually stable framing across diverse poses and body shapes.

In addition to the rendered images, we export the corresponding SOMA mesh. We then convert it into an SMPL-X using a pre-computed regression matrix, followed by a parameter inversion step in which we optimize the SMPL-X parameters via trust region newton conjugate gradient method [61] to best match the converted mesh. We show samples from the rendered dataset in Fig. 13.

B.2. Generative Branch

B.2.1. Semantic Factorization

We construct a factorized latent space by decomposing the generative prior into semantically meaningful axes. For each factor, we curate a dedicated vocabulary that captures its underlying variation (e.g., appearance attributes, scene composition, or stylistic cues). These vocabularies collectively define controllable semantic directions along which data diversity can be systematically spanned. These vocabularies are automatically expanded using GPT-5 to ensure broad coverage while preserving the semantic purity of each factor.

- *Actions* have 131 carefully constrained micro-gestures grouped implicitly (speaking, explanatory, facial, grooming, fit-check) and phrased as short dynamic–return patterns to stabilize temporal synthesis while avoiding occlusion or exaggerated motion.
- *Hair* splits into 26 natural color variants and 54 face-visible styles spanning length, texture, braids, locs, curls, and updos.
- *Lighting control* uses 27 daylight and 25 night or practical scenario words plus 22 declarative reinforcement lines to couple physically plausible cinematography (direction, diffusion, key/fill balance, rim separation) with exposure stability (“Exposure anchors on the face”, “Shadow detail is preserved”).
- *Outfit* is factored into orthogonal granularities: 64 balanced color tones (8 groups \times 8 hues), 45 fabric/material descriptors, a large library of tops (>400) and outerwear (>1000) with an optional ‘None’ sentinel for absence, plus 45 accessories likewise optionally omitted. Surface semantics are isolated into micro pattern sets (woven, knit, formal micro-structures), small neutral wordmarks, a large bank of mid-scale front graphics (>300 non-branded, stylized motifs), all-over prints, color-blocking schemes, embroidery/appliqué types, and extensive outerwear construction/detail modifiers (>200).
- *Role* and attire archetypes form the largest axis (>1000 unique descriptors) spanning contemporary professions, protective gear, historical armors, global traditional garments, performing arts, subcultures, sports kits, speculative sci-fi, fantasy and genre motifs, craft and maritime occupations, emergency and technical variants—each phrase bundling a silhouette anchor plus distinctive accessories for high visual discriminability while remaining culturally neutral.
- *Subjects* provide 24 age granularity words (coarse bands plus early/mid/late decades), 52 region-level origin abstractions (continental and sub-regional without nationality specificity), and inclusive gender nouns (“man”, “woman”, “person”, “non-binary person”), intentionally

broad to mitigate bias.

- *Time* contributes 26 day/night or twilight states (“golden hour”, “civil twilight after sunset”, “dawn blue hour”) paired with a coarse day/night flag, directly complementing lighting vocabulary to steer chromatic and contrast regimes.

B.2.2. Scene Composition

Given the factorized vocabularies defined above, we next compose them into complete scene descriptions that serve as conditioning signals for the upper-body video generator. Rather than relying on free-form textual prompts, we programmatically assemble each scene by sampling a small set of descriptors along the active semantic axes—such as subject identity cues, actions, hairstyle, lighting setup, outfit or role, and time-of-day—and inserting them into a structured scene template. This approach ensures that every generated instance is grounded in the same underlying factor space while still exhibiting rich and controlled visual diversity.

To further broaden the appearance distribution, we introduce two complementary scene-composition regimes that differ in how clothing-related factors are instantiated. These regimes share the same semantic axes but emphasize distinct clothing conventions, allowing us to explore a wider range of apparel variability without altering the core factorization.

- **Outfit-centric composition.** In this regime, the scene description is constructed by foregrounding the explicit outfit-related vocabulary—including color palettes, fabric types, garment categories (e.g., tops, outerwear), accessories, and surface patterns—while deliberately leaving the “role” attribute unspecified. This strategy encourages the generator to synthesize visually clean and relatively simple garments that are easier to segment, normalize, and analyze. It also provides more disentangled control over low-level appearance attributes by isolating clothing factors from higher-level semantic cues. The corresponding outfit-centric template is shown below:

{time_of_day}, *{lighting}*, *{shot_size}*, *center composition. A/An {age} {gender_noun} (from {region}) wearing a {top_color} {top_fabric} {top} with/featuring {top_decoration} paired with a {outer_color} {outerwear} {outerwear_detail} and {accessory}, with {hair_color} {hairstyle}. The person {action}, in a waist-up, standing, fixed-camera shot with arms and hands visible; lighting remains stable and physically plausible.*

- **Role-centric composition.** In this regime, the scene description is anchored on the rich role–attire archetype axis, which provides high-level cues about profession, social persona, cultural style, or situational context. Once a role is selected, the remaining factors—such as subject attributes, action, hairstyle, lighting, and time-of-day—are sampled to remain semantically compatible

with the chosen archetype. Because each role phrase implicitly encodes a characteristic silhouette, associated accessories, and distinctive detailing, this strategy naturally produces outfits with more elaborate structure and heightened stylistic diversity compared with the outfit-centric scheme.

{time_of_day}, {lighting}, {shot_size}, center composition. A/An {age} {gender} {role} from {region}, wearing characteristic {role}-specific clothing and accessories, with {hair_color} {hairstyle}. The person {action}, in a waist-up, standing, fixed-camera shot with arms and hands visible; lighting remains stable and physically plausible.

A corresponding negative description is constructed in the same manner by sampling several terms from a curated list of undesired artifacts (e.g., low resolution, motion jitter, flicker, over- or under-exposure, extreme torso crops, seated or occluded poses). Aside from this auxiliary negative specification, the two scene-composition strategies share an identical sampling pipeline; they differ solely in how clothing-related information is selected, emphasized, and integrated into the final scene description.

B.3. Filmic Realism Regularization

The factorized samplers introduced above produce scene descriptions that are structurally clean and fully disentangled across semantic axes, but the resulting text is intentionally minimal. In the outfit-centric regime, such terseness is acceptable: the specification primarily consists of low-level, compositional attributes—colors, fabrics, garments, simple actions—and can already drive the generator to produce plausible videos. In contrast, the role-centric regime operates at a much higher semantic level. A single role indicator implicitly encodes equipment, safety constraints, cultural context, and a characteristic visual grammar. Directly combining these role cues with independently sampled attributes often results in descriptions that are grammatically valid yet visually implausible or internally inconsistent (e.g., “a firefighter in full bunker gear with long, loose hair flowing over the shoulders”).

This mismatch highlights a key insight in our data design: *semantic factorization alone does not guarantee filmic coherence*. High-level roles impose structured dependencies among appearance, action, accessories, and physical context—dependencies that must be restored for the compositions to resemble real-world footage. To address this, we leverage a lightweight language-model-based postprocessor that acts as a *filmic realism regularizer*. Given a structured template as input, the instruction-tuned Qwen-Instruct-14B [78] rewrites the description into a fluent, naturalistic scene while preserving all controllable factors introduced by the sampler. As illustrated in Fig. 14, the model

performs three key types of corrections:

- **Disambiguation.** Remove or resolve ambiguous phrasing in the compositional template (e.g., clarifying vague actions or lighting descriptions) so that a single, concrete visual interpretation is implied.
- **Role-aware scene completion.** For role-centric compositions, insert an appropriate surrounding scene or objects that are compatible with the specified role (e.g., adding a station, workplace, or tools) and remove attribute combinations that contradict typical equipment or safety requirements.
- **Richer clothing detail.** Elaborate the clothing description with additional but compatible details and surface patterns (e.g., stitching, pockets, insignia, emblems), increasing visual complexity without changing the underlying factors selected by the sampler.

B.4. Video Generation

The refined scene descriptions are then fed into the Wan2.2-TI2V-5B [80] model, using its default inference configuration to synthesize upper-body video clips. The generator directly produces short sequences that inherit both the structured control from our factorized sampler and the filmic coherence enforced by the realism regularizer. Representative results for the two composition regimes are shown in Fig. 15 and Fig. 16, which display the masked and cropped outputs for the outfit-centric and role-centric settings, respectively.

B.5. Side/Back View Completion

In practice, Wan2.2-TI2V-5B does not always produce stable, identity-consistent samples when a single person turns in place or rotates themselves. To supplement the multi-view supervision, we therefore perform simple side/back-view synthesis with Qwen-Image-Editing [79]: for each generated clip, we randomly sample one frame as the reference image and ask the model to generate left, right, and back views of the same subject. We use the following prompts for side and back views:

Side view: “Change the subject to a left 90° pure side profile (camera-left, yaw≈ +90°). Preserve identity (facial proportions/shape), hair length & color, clothing color & material, body height & build; keep lighting direction/intensity consistent; do not change the background or composition. Photo-realistic, high resolution.”

Back view: “Without changing the person’s identity or composition, rotate the subject to a back-facing viewpoint (≈ 180°). Preserve height, body shape, hair length & color, clothing color & material, and accessory positions; keep lighting direction/intensity consistent; maintain the background’s texture and perspective as much as possible. The back view should be

physically consistent with the front (collar shape, fabric folds, hair volume, shoulder line). Photo-realistic, high resolution.”

Guiding an image-editing model to rotate a person to a side-view using textual prompts is not always reliable. We empirically find that the success rate can be significantly improved by adopting a simple strategy: we always use a single side-view prompt, and obtain right-view samples by horizontally flipping the reference image before editing and flipping the edited result back afterward. This allows both left and right side views to be generated using the same textual prompt. The augmented dataset is illustrated in Fig. 17. Although the resulting poses are not strictly consistent with those in the input images, this mismatch is acceptable because our training is formulated over reference–target pairs.

B.6. Discussion

Our data pipeline is intentionally simple, and the model design remains lightweight, leaving substantial room for future enhancement. Because the realistic-style supervision views in our synthetic corpus mainly cover side and back angles, side-view supervision may cause Gaussians on the supervised side to attenuate due to projections from the opposite side. The generative data may also produce imperfect hand geometry, occasionally resulting in floating points around the fingers. In addition, the projection-based scattering and decoder inpainting introduce a natural transition between observed and unobserved regions. These aspects point to several promising directions, such as enriching supervision viewpoints, improving hand priors, or incorporating GAN-based or DPT-style refinement for smoother cross-view consistency. Nevertheless, even with this minimalistic design, our synthetic data pipeline and dual-UV model deliver faithful reconstructions, robust generalization across head/half/full-body inputs, and plausible novel-view synthesis, achieving state-of-the-art or highly competitive performance.

C. Details of Proxy Mesh Estimation

In the following, we introduce our proxy mesh estimation pipeline, which we will refer to as *the tracker*. The overall workflow of our tracker is illustrated in Fig. 10. Our tracker is designed to produce stable estimates for less-restricted inputs. We use SMPL-X to represent the full body, FLAME to represent the head, and MANO to parameterize hands.

For SMPL-X, we parameterize the body with shape coefficients $\beta^{\text{smplx}} \in \mathbb{R}^{N_\beta}$, expression coefficients $\psi^{\text{smplx}} \in \mathbb{R}^{N_\psi}$, pose coefficients

$$\theta = [\theta^{\text{glob}}, \theta^{\text{body}}, \theta^{\text{lhand}}, \theta^{\text{rhand}}, \theta^{\text{jaw}}] \in \mathbb{R}^{3K},$$

and a global translation vector $\mathbf{t} \in \mathbb{R}^3$. For FLAME, we use shape coefficients $\beta^{\text{flame}} \in \mathbb{R}^{N_\beta}$, expression coefficients

$\psi^{\text{flame}} \in \mathbb{R}^{N_\psi}$, and head pose coefficients $\theta^{\text{flame}} \in \mathbb{R}^{3K_{\text{flame}}}$. For MANO, we denote the MANO shape coefficients by $\beta^{\text{mano}} \in \mathbb{R}^{N_\beta^{\text{hand}}}$, the hand pose coefficients by $\theta^{\text{mano}} \in \mathbb{R}^{3K_{\text{hand}}}$, and the hand translation by $\mathbf{t}^{\text{mano}} \in \mathbb{R}^3$. In practice, MANO is instantiated separately for the left and right hands (with parameters $\theta^{\text{mano,l}}, \theta^{\text{mano,r}}$, etc.). Given a subject, we share the shape across time and models, i.e., all frames of the same video share the same SMPL-X and FLAME shape coefficients.

Previous trackers exhibit limitations under our setting. The LHM tracker cannot capture expressive facial motion and performs poorly for upper-body or shoulder-up crops. The GUAVA tracker achieves accurate results under the strict assumption that both hands and face are visible. However, when hands are occluded or truncated, GUAVA tracker often produces unstable and unpredictable estimates.

C.1. Initial Estimates

We first consider off-the-shelf human mesh recovery models for obtaining an initial solution from the input frame. PIXIE [20] is a classic multi-stage model that crops out the face, hands, and body and processes them with dedicated encoders, whose features are then jointly fused. However, when one or both hands are not visible, its hand estimates become highly unreliable as shown in Fig. 11, which also explains why GUAVA focuses on frames where both hands are visible.

In contrast, ViT-based methods such as Multi-HMR [3] do not require explicit face or hand crops. Nevertheless, in frames where the hands are not visible, they often default to placing the hands near the bottom of the image, presumably due to dataset bias. OSX [54], a one-stage model trained on upper-body data, does not suffer from this issue. This behavior is demonstrated in Fig. 12. Therefore, in our tracker we implement both Multi-HMR and OSX: Multi-HMR is used for full-body inputs, while OSX is used for upper-body inputs. Since our curated dataset mostly contains upper-body views, We mainly use OSX in preprocessing.

C.2. FoV Correction

Methods such as OSX are trained under a very narrow FoV assumption ($\approx 2^\circ$), which approximates the perspective projection with an orthographic one. While this is helpful for recovering a stable 3D pose from a single image, it introduces large uncertainty when anchoring 3D Gaussians on the SMPL-X mesh. Given an input frame, after obtaining an initial SMPL-X estimate from OSX, we first convert the camera intrinsics and the mesh translation along the z -axis to a canonical FoV of 30° .

Let (f_x, f_y) denote the original focal lengths and c_x the principal point in the horizontal direction. We compute a new focal length f'_x based on the desired FoV and define

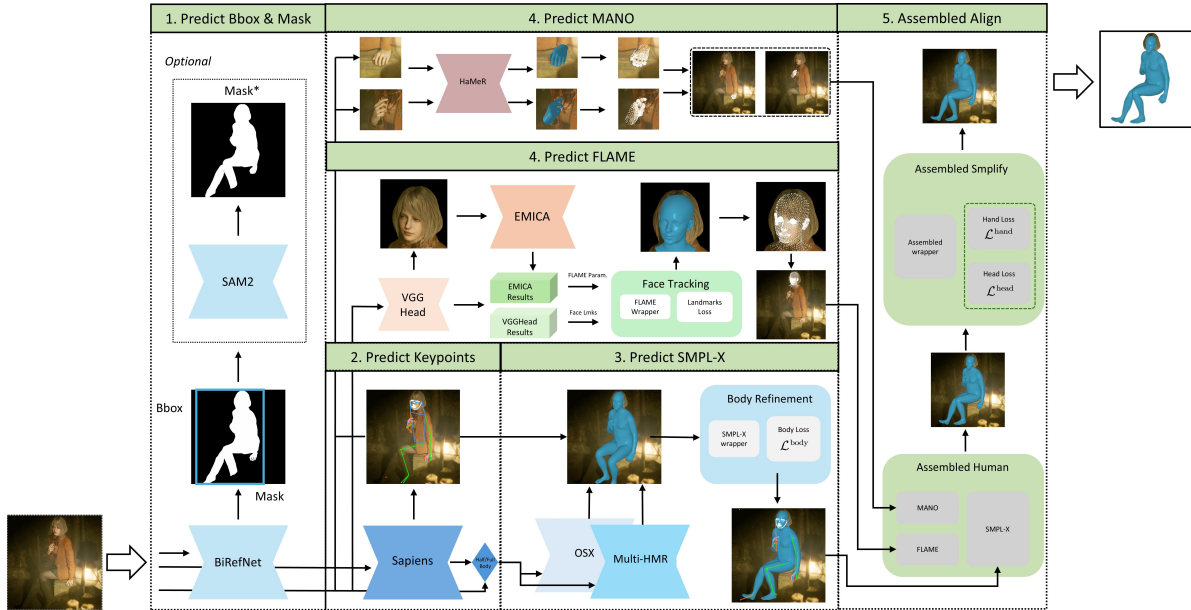


Figure 10. **Estimation Pipeline Diagram.** We illustrate our proxy-mesh estimation pipeline using a single image for clarity, while noting that the pipeline naturally supports parallel processing for multi-frame inputs. Starting from an input image, we preprocess it to extract a foreground mask and apply a pretrained human mesh recovery model to obtain an initial mesh estimate. The initial estimate is subsequently refined through body, head, and hand refinement.



Figure 11. **Hands Missing Prediction.** Multi-stage methods, such as PIXIE, often produce unpredictable results when hand regions are missing.



Figure 12. **Multi-HMR and OSX.** We find that OSX, trained primarily on upper-body data, produces reasonable results when hands are not visible, whereas MultiHMR often yields unsatisfactory predictions.

the scaling factor

$$s_x = \frac{f'_x}{f_x}. \quad (18)$$

To preserve the aspect ratio, we set $f'_y = s_x f_y$. We also update the depth translation using the same scale, i.e., $t'_z = s_x t_z$.

C.3. Optimization

Body Refinement. Using this canonicalized camera, we back-project Sapiens 2D keypoints to the 3D mesh and optimize the global orientation θ^{glob} , body pose θ^{body} , hand poses $\theta^{\text{lhand}}, \theta^{\text{rhand}}$, and translation \mathbf{t} . This first stage aligns the SMPL-X mesh to the input frame with the following objective:

$$\begin{aligned} \mathcal{L}^{\text{body}} = & \lambda_{\text{reproj}} \mathcal{L}_{\text{gmof}}(K, \hat{K}) + \lambda_{\text{mask}} \mathcal{L}_{\text{mask}}(M, \hat{M}) \\ & + \lambda_{\text{reg}} \mathcal{L}_{\text{reg}} + \lambda_{\text{up}} \mathcal{L}_{\text{up}} + \lambda_{\text{smo}} \mathcal{L}_{\text{smo}}, \end{aligned} \quad (19)$$

where $\mathcal{L}_{\text{gmof}}$ is the Geman–McClure robust loss [4]. The set K contains 2D Sapiens keypoints, and \hat{K} are the re-projected keypoints from SMPL-X. In this stage we use all head, body, and hand keypoints whose confidence is larger than 0.6. Empirically, we observe that when the person stands with arms down, with hands invisible but forearms still visible, the predicted wrist locations are unstable and often flip upwards, which misleads the optimization. Therefore, for upper-body inputs we ignore the left and right wrist keypoints when optimizing the body. M is the foreground mask obtained during preprocessing, and \hat{M} is the rendered silhouette of the SMPL-X mesh; $\mathcal{L}_{\text{mask}}$ encourages \hat{M} to lie inside M . \mathcal{L}_{reg} regularizes the current pose to stay close to the initial estimate. For upper-body inputs, we set $\lambda_{\text{up}} > 0$ and define \mathcal{L}_{up} to encourage the direction vector from the pelvis to the neck to be aligned with the vertical axis, correcting the front-leaning or backward-leaning poses caused by depth ambiguity in OSX. When optimizing multiple consecutive frames jointly, \mathcal{L}_{smo} is defined as the second-order temporal difference of the projected 2D mesh vertices to reduce jitter.

FLAME Refinement. For video frames or single images, we integrate the GAGAvatar [16] tracking pipeline to obtain FLAME estimates. Note that all frames in a video share the same FLAME shape β^{flame} and the same SMPL-X shape β^{smplx} . After obtaining FLAME predictions (shape β^{flame} , expression ψ^{flame} , and pose θ^{flame}), we estimate an affine transformation that aligns the canonical SMPL-X head to the predicted FLAME head, then replace the SMPL-X head vertices with the FLAME head before perform linear blend skinning. If the FLAME tracking fails for a frame (e.g., facial landmarks detect failed), we fall back to using a zero FLAME parameter as a dummy input.

We further refine the head by leveraging the dense FLAME re-projection like GUAVA tracker:

$$\begin{aligned} \mathcal{L}^{\text{head}} = & \lambda_{\text{head}} \mathcal{L}_{\text{gmof}}(V_{\text{head}}, \hat{V}_{\text{head}}) \\ & + \lambda_{\text{reproj}} \mathcal{L}_{\text{gmof}}(K, \hat{K}) \\ & + \lambda_{\text{mask}} \mathcal{L}_{\text{mask}}(M, \hat{M}) + \lambda_{\text{reg}} \mathcal{L}_{\text{reg}} \\ & + \lambda_{\text{up}} \mathcal{L}_{\text{up}} + \lambda_{\text{smo}} \mathcal{L}_{\text{smo}}, \end{aligned} \quad (20)$$

where V_{head} and \hat{V}_{head} denote the dense head vertices from FLAME and SMPL-X in image space, respectively. In this stage we optimize the SMPL-X pose and translation ($\theta^{\text{glob}}, \theta^{\text{body}}, \theta^{\text{lhand}}, \theta^{\text{rhand}}, \mathbf{t}$) as well as the FLAME shape and expression ($\beta^{\text{flame}}, \psi^{\text{flame}}$). The keypoint loss only supervises body keypoints in this stage.

Hand Refinement. Finally, we refine the hand regions. If the hands in the input are usable, we run HaMeR [67] to estimate MANO parameters, from which we obtain dense hand keypoints and hand poses. When valid hand poses are available, we update the SMPL-X hand poses $\theta^{\text{lhand}}, \theta^{\text{rhand}}$ accordingly and perform a dedicated hand refinement with the objective

$$\begin{aligned} \mathcal{L}^{\text{hand}} = & \lambda_{\text{hand}} \mathcal{L}_{\text{gmof}}(V_{\text{hand}}, \hat{V}_{\text{hand}}) \\ & + \lambda_{\text{head}} \mathcal{L}_{\text{gmof}}(V_{\text{head}}, \hat{V}_{\text{head}}) \\ & + \lambda_{\text{reproj}} \mathcal{L}_{\text{gmof}}(K, \hat{K}) + \lambda_{\text{mask}} \mathcal{L}_{\text{mask}}(M, \hat{M}) \\ & + \lambda_{\text{reg}} \mathcal{L}_{\text{reg}} + \lambda_{\text{up}} \mathcal{L}_{\text{up}} + \lambda_{\text{smo}} \mathcal{L}_{\text{smo}}, \end{aligned} \quad (21)$$

where V_{hand} and \hat{V}_{hand} denote the dense hand vertices in image space. In this stage we also optimize the SMPL-X poses of the wrists, shoulders, and elbows, while the keypoint loss supervises body and hand keypoints.

All three optimization stages use the Adam [41] optimizer with a learning rate of 10^{-3} . For additional implementation details, please refer to our released code.

Non-frontal Case. Estimating SMPL-X parameters for side and back views generated by Qwen-image is particularly challenging, due to the lack of suitable pretrained models and supervision signals in these viewpoints. Fortunately, these Qwen-generated side and back views are typically pose-neutral and almost perfectly aligned to $\pm 90^\circ$ and 180° viewpoints. We therefore introduce several tailored modifications when tracking Qwen-edited images.

For side views, we enforce the direction vectors between left and right ears, left and right shoulders, and left and right hips to be parallel to the camera viewing direction. We disable the additional FLAME refinement and instead directly use Sapiens facial keypoints for optimization, because we

Table 3. Hyperparameters used for the three tracking stages.

Hyperparameter	Value
$\lambda_{\text{reproj}}(\mathcal{L}^{\text{body}})$	10^2
$\lambda_{\text{reproj}}(\mathcal{L}^{\text{head}})$	10^2
$\lambda_{\text{reproj}}(\mathcal{L}^{\text{hand}})$	10^1
$\lambda_{\text{reg}}(\mathcal{L}^{\text{body}})$	10^2
$\lambda_{\text{reg}}(\mathcal{L}^{\text{head}})$	10^2
$\lambda_{\text{reg}}(\mathcal{L}^{\text{hand}})$	10^1
λ_{mask}	10^2
λ_{up}	10^4
$\lambda_{\text{smo}}(\mathcal{L}^{\text{body}})$	5×10^2
$\lambda_{\text{smo}}(\mathcal{L}^{\text{head}})$	5×10^4
$\lambda_{\text{smo}}(\mathcal{L}^{\text{hand}})$	5×10^5
λ_{head}	10^3
λ_{hand}	10^2

observe that the GAGAvatar tracking pipeline tends to produce a noticeable tilt for $\pm 90^\circ$ side views. Moreover, during the first body optimization stage, we do not optimize the global translation. If translation is updated in this stage, the dense facial landmarks tend to pull the entire pose towards cases with a protruding neck.

For back views, reliable landmarks are largely unavailable. In this case, we mainly rely on the silhouette loss $\mathcal{L}_{\text{mask}}$ and the upright prior \mathcal{L}_{up} to obtain a plausible SMPL-X configuration.

Summary Our tracker is designed for the general case: it aims to provide stable estimates under diverse input conditions, thereby enabling us to scale up our dataset reliably. We present qualitative comparisons with the LHM and GUAVA trackers in Fig. 18. The LHM tracker fails to produce correct results in certain cases, while the GUAVA tracker can estimate accurately when both hands are clearly visible. In contrast, our tracker delivers robust performance across a wide range of input conditions.

D. Ethic Statement

The use of synthetic data for 3D human avatar reconstruction offers promising advancements in digital representation and interaction. However, this technology also raises several ethical concerns. While synthetic data reduces the risk of privacy violations associated with personal information, it still presents potential risks in terms of misuse. The ability to generate realistic 3D avatars may be exploited for creating deceptive content, such as deepfakes, leading to identity theft, fraud, or harassment. Moreover, the potential for real-time animation of avatars could contribute to the spread of misinformation or online manipulation. It is critical to ensure that the technology is used responsibly, with trans-

parent processes in place to detect and prevent malicious use. Informed consent and clear communication about the synthetic nature of data should be emphasized, even if no personal data is directly involved. Furthermore, measures should be taken to secure the technology against unauthorized access and misuse, while fostering public awareness and trust in these systems.

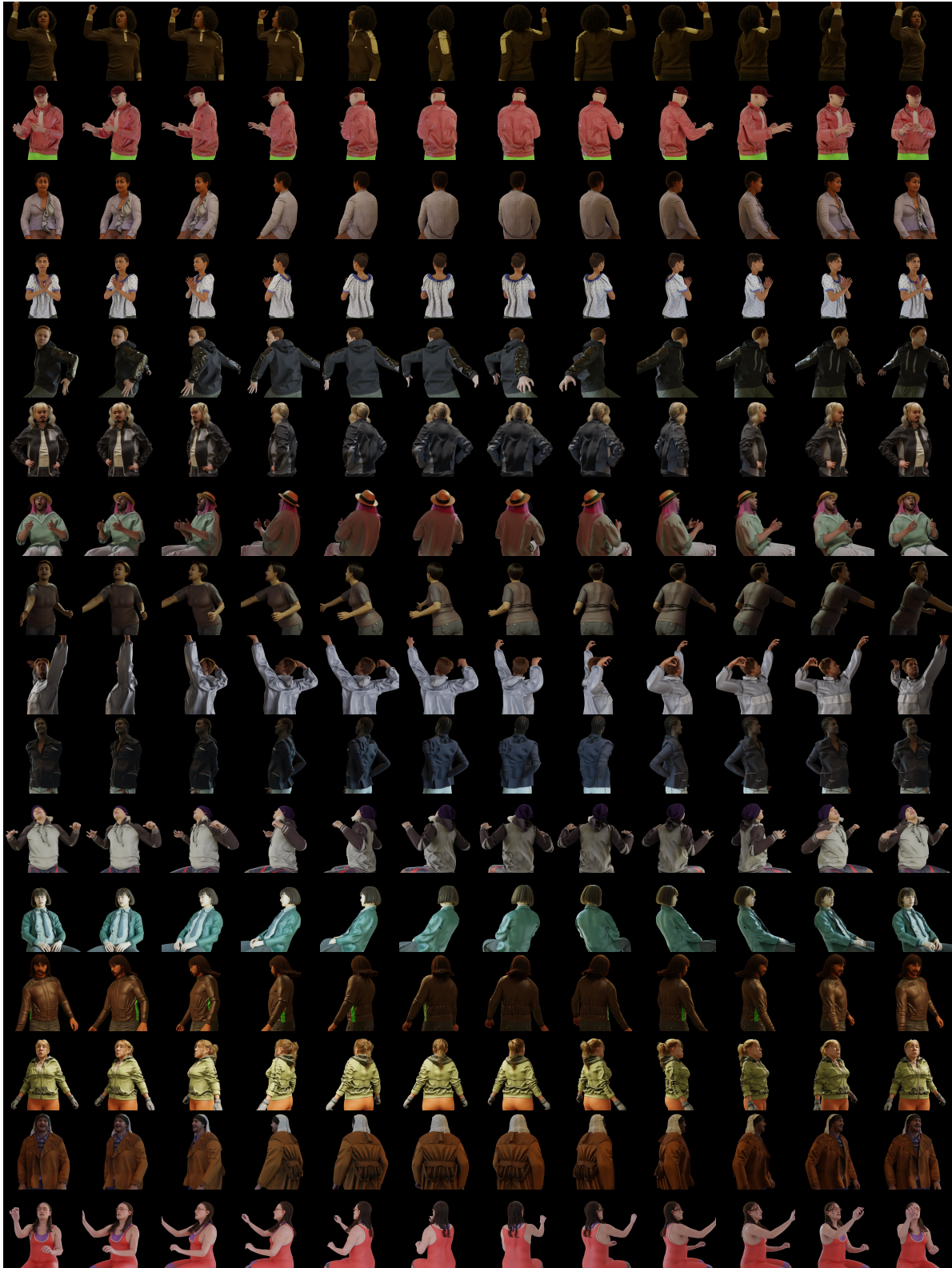


Figure 13. **Synthetic Rendering Dataset.** Our synthetic rendering dataset contains diverse body poses, rendered from multiple viewpoints with perfect mesh annotations, providing strong structural priors for model training.

System Prompt for Realism Regularizer

You are a film director and realism regularizer for text-to-video prompts. Given a structured but terse English prompt, rewrite it into a fluent, cinematic description while preserving all factual attributes (subject, role, clothing, actions, time, lighting). The output must be in English.

[Global Framing Lock — highest priority]

- Enforce a half-body, waist-up view unless the input explicitly asks for full body or extreme close-up.
- State clearly: waist-up or half-body framing, natural perspective (no wide-angle distortion), camera level, steady framing, consistent exposure, comfortable headroom and armroom.
- Explicitly avoid: full-body framing, feet or knees in frame, and extreme head-only close-ups.
- If there is motion, keep the same half-body viewpoint.

[Main objectives]

1. Cinematic completion

- Optionally add up to four concise cinematic attributes: time of day, light source/quality/direction, color tone, shot size, camera angle, and composition.
- Do not contradict existing camera or style hints in the input.

2. Realism and disambiguation

- Resolve ambiguous phrasing so that the scene has a single, concrete interpretation.
- For role-centric prompts, make the outfit, equipment, and environment realistic for that role (e.g., firefighter, doctor, pilot), and remove clearly implausible combinations (such as unsafe hair or gear for that role).
- Add a short, coherent background description that matches a waist-up shot (1–3 visible elements, no brands or readable text).

3. Clothing detail and patterns

- For non-uniform outfits, enrich the upper-body clothing with a few large-scale, clearly visible graphics or patterns (e.g., big illustration, bold geometric blocks, abstract emblem, or non-brand letter/number logo), and specify placement and 3–5 main colors.
- For strict uniforms or protective gear, keep the typical design and colors; you may add only generic patches, stripes, or abstract logos, or move larger decorative elements to accessories or background posters.
- Ensure large prints are clearly visible within the waist-up frame.

[Style, motion, and safety]

- If the input has a style, keep it; otherwise, do not invent a strong new style.
- Refine any actions into natural, moderate motions (e.g., slight turn, adjusting clothing, gesturing while speaking) without breaking the framing.
- If the input contains sexual, explicit, or otherwise unsafe content, REPLACE it with a completely safe, aesthetically pleasing scenario instead of refusing.

Output: a single rewritten prompt in English, 60–200 words, without any meta-commentary or prefixes.

Figure 14. **Filmic Realism Regularization.** The structured templates are processed by a lightweight LLM that improves linguistic fluency and resolves inconsistencies, yielding scene descriptions with enhanced realism and contextual coherence.



Figure 15. **Outfit-centric Generation.** Generation guided by outfit produces visually coherent and structurally consistent human images.



Figure 16. **Role-centric Generation.** Role-guided composition produce human images with noticeably more complex textures and styles.



Figure 17. **Side/Back-view Augmentation.** We leverage advanced image-editing models to supplement abundant side- and rear-view information.



Figure 18. **Proxy Mesh Estimation.** We showcase how our tracker, GUAVA, and LHM perform on arbitrary upper-body images, highlighting the robustness under unconstrained input conditions.